SETUP AND CALIBRATION OF A HETERODYNE RECEIVER FOR MICROWAVE SENSORS

A Thesis Submitted to
the Graduate School of Engineering and Sciences of
İzmir Institute of Technology
in Partial Fulfillment of the Requirements for the Degree of

MASTER OF SCIENCE

in Electrical and Electronics Engineering

by
Saygın BİLDİK

July 2008
İZMİR

We approve the thesis of **Saygın BİLDİK**

_____

Assist. Prof. Dr. Sevinç AYDINLIK BECHTELER
Supervisor

_____

Assoc. Prof. Dr. Thomas F. BECHTELER
Committee Member

_____

Assist. Prof. Dr. Alp KUŞTEPELİ
Committee Member

_____**16 JULY 2008**_____
Date

_____   _____
Prof. Dr. F. Acar SAVACI   **Prof. Dr. Hasan BÖKE**
Head of the Department of Electrical   Dean of the Graduate School of
and Electronics Engineering   Engineering and Science

ACKNOWLEDGEMENTS

ABSTRACT

SETUP AND CALIBRATION OF A HETERODYNE RECEIVER FOR MICROWAVE SENSORS

The demand for sensors for the measurement of various quantities has increased with the automatisation of industrial processes. In many cases microwave techniques provide competitive solutions. A large number of important applications are found such as dielectric constant measurement, moisture measurement, length measurement, leaking gas detection, radar applications, etc.

Heterodyne receiver system is set up and calibrated to measure the resonant frequencies of resonator type sensors precisely and inexpensively. Output frequencies of the resonator type sensors are varied by the change in physical dimensions of the resonator or physical properties of a material placed in a resonator to be processed. Instead of the classical audio amplifier and a loudspeaker which are the elements of a classical heterodyne receiver, a frequency counter evaluates the signal. Thus, the heterodyne receiver used in frequency measurement system consists of a mixer, a voltage controlled oscillator, a microstrip line low-pass filter and a frequency counter. The output signal of the resonator is converted down to an intermediate frequency which is in the counting range of frequency counter via the mixer with VCO. Then, the measured data is sent to a computer and it is converted to the wanted data related to which measurement (distance, dielectric constant, etc.) is done and which resonator is used.

In this study, distance measurement is performed by using a circular groove guide oscillator as a microwave sensor connected to the heterodyne receiver system. The most important feature of the groove guide oscillator is its resonator consists of physically two open parallel plates. Therefore, the resonant frequency of the oscillator can be changed depending on the distance between the two parallel plates. This makes the groove guide oscillator feasible for some applications like the distance measurement, using the resonant frequency measurement setup.

ÖZET

MİKRODALGA SENSÖRLERİ İÇİN HETERODİN ALICI KURULUMU VE KALİBRASYONU

Çeşitli niceliklerin ölçülmesi için kullanılan sensörlere olan talep endüstriyel işlemlerin otomasyonu ile birlikte artmıştır. Birçok durumda mikrodalga teknikleri rekabetçi çözümler sunmaktadır. Bu hususta dielektrik sabiti ölçümü, nem ölçümü, uzunluk ölçümü, gaz kaçağı tespiti ve radar uygulamaları gibi birçok önemli uygulamalar yapılmaktadır.

Rezonatör tipi sensörlerin rezonans frekanslarının, hassas ve ucuz olarak ölçülmesi için heterodin alıcı sistemi kurulmuş ve ölçümlenmesi yapılmıştır. Rezonatör tipi sensörlerin çıkış frekansları rezonatörün fiziksel boyutlarının değişimine göre ve rezonatörün içine ölçüm yapılması için yerleştirilen maddenin fiziksel özelliklerine göre değişmektedir. Sinyalin değerlendirilmesi, klasik heterodin alıcının elemanlarından olan ses yükselticisi ve hoparlörün yerine, frekans sayıcı tarafından yapılmaktadır. Böylece, frekans ölçüm sisteminde kullanılan heterodin alıcı, karıştırıcı, voltaj kontrollü osilatör, mikroşerit hatlı alçak geçiren filtre ve frekans sayıcıdan oluşmaktadır. Rezonatörün çıkış frekansı, karıştırıcı vasıtasıyla, frekans sayıcının ölçüm aralığına uygun olarak bir ara frekansa düşürülür. Daha sonra, ölçüm değeri bir bilgisayara gönderilir ve hangi ölçümün (mesafe, dielektrik sabiti, vs.) yapıldığına ve hangi rezonatörün kullanıldığına göre istenen bilgiye dönüştürülür.

Bu çalışmada, mikrodalga sensörü olarak heterodin alıcı sistemine bağlı olan aktif dairesel oyuklu dalga kılavuzu osilatörü kullanılarak mesafe ölçümü yapılmıştır. Oyuklu dalga kılavuzu osilatörünün en önemli özelliği rezonatör yapısının açık ve ayarlanabilir olmasıdır. Bundan dolayı, rezonatör aralığının boyu değiştirildiğinde osilatörün rezonans frekansı değişmektedir. Bu da bize, oyuklu dalga kılavuzu rezonatörü ile rezonans frekansı ölçüm sistemini kullanarak mesafe ölçümü gibi değişik uygulamalar yapmaya olanak sağlayacaktır.

TABLE OF CONTENTS

LIST OF FIGURES

LIST OF TABLES

CHAPTER 1

INTRODUCTION

Sensors are devices that convert a physical quantity into a signal carrying information. According to the nature of the signal, a sensor can be characterized as electrical, mechanical, optical and microwave. The demand for sensors for the measurement of various quantities has increased with the automatisation of industrial processes. In many cases microwave techniques provide competitive solutions. A large number of important applications are found such as dielectric constant measurement, moisture measurement, length measurement, particle flow control in pipes, leaking gas detection, level of liquids or gases in the tanks, speed measurement, radar applications, etc. The basic method for all of these applications is converting nonelectrical quantities to electrical quantities at microwave frequencies. This method relates electromagnetic wave quantities (frequency, field intensity, polarization, wave velocities and impedance) to desired nonelectromagnetic physical quantities (dimensions, speed, etc.) or electromagnetic properties of the medium (permittivity, permeability, etc.) to desired nonelectromagnetic physical properties of the medium (moisture, density, etc). The capabilities to perform measurements nondestructively without contact from a short distance, using penetrating waves without health hazards to a person are general advantages of microwave sensors. The significant drawback is the effect of several variables such as temperature, density, moisture during the microwave measurement. However, microwave sensors show better performance than optical sensors under dust, dirt, rain, fog, snow, etc.

Microwave sensors can be divided into four groups: resonator type sensors, transmission type sensors, radiometers, and radars. In resonator type sensors the material to be processed is placed in a resonator and its physical properties of such as moisture, density, composition, etc. cause a change in the resonant frequency. Furthermore, the change in the physical dimensions of resonator also shifts the resonant frequency. The process of transmission type sensors is propagation of microwaves through a material by using a transmitter and a receiver. Here, the measured value is the attenuation or the phase shift caused by the material and it is used to determine the electrical characteristics of the material. Microwave radiometers measure thermal microwave noise power radiated

by a target. The physical temperature and surface characteristics of the target affects the radiated power from the material. Radars measure the reflection and scattering of electromagnetic waves from a target and the measurement of movement, speed, distance, vibration, etc. are determined from these data.

The aim of this study is to measure the resonant frequency of resonator type microwave sensors inexpensively and precisely. In order to provide low-cost and precise measurement a heterodyne receiver is set up and calibrated according to the resonator used. The invention of heterodyne receiver dates back to the early part of 1918 (Armstrong 1921, Armstrong 1924). The goal of the invention was to amplify short wave signals for experimental radar applications and long distance reception from broadcasting stations. Therefore, the heterodyne receiver system is modified to use the receiver for the frequency measurement. The heterodyne system used in this thesis consists of a mixer, a voltage controlled oscillator, a microstrip line low-pass filter and a frequency counter operating up to 2.5 GHz. The output signal of the resonator is converted down to an intermediate frequency which is appropriate to the counting range of frequency counter via the mixer with VCO. Then, the measured data is sent to a computer and it is converted to the wanted data related to which measurement (distance, dielectric constant, etc.) is done and which resonator is used. Therefore, calibration of the system is necessary for each resonator that is used at the sensor side. In addition, a filter is used to suppress the unwanted signals beyond the intermediate frequency.

For active resonators, generally spectrum analyzers are used to measure the frequency of resonators. Furthermore, for passive resonators, a MMIC device and digital signal processing unit (Megej, et al. 2002) or reference signal (excitation signal of the resonator) comparison by a mixer and microprocessor unit (Carullo, et al. 1999) with signal generators are used to measure the frequency of the resonator. Using spectrum analyzers or network analyzers to measure the variable resonant frequency of resonators and using signal generators for the excitation of passive generators increase the cost. Thus, a heterodyne receiver system decreases the cost and works as precisely as the other systems.

In this study, distance measurement is performed by using a circular groove guide oscillator (Aydinlik, et al. 1996) as a microwave sensor connected to the heterodyne receiver system. The frequency information (output of the frequency counter) is received and converted to the distance value via a computer. The main and most important feature

of the groove guide oscillator is that, its resonator consists of physically two open parallel plates. Therefore, the resonant frequency of the oscillator can be changed depending on the distance between the two parallel plates. This makes the groove guide oscillator feasible for some applications like distance measurement, using the resonant frequency measurement setup. When the distance is calibrated with respect to the resonant frequency of the oscillator, the system can be used as a distance measurement system.

The distance measurement system is presented in Chapter 2. Chapter 3 describes the principle of the heterodyne system. The design of the microstrip line filter, tests of the each receiver element and conversion of the frequency information to the distance data are stated in Chapter 4. Finally, the conclusions about the study and the future work are given in the last chapter.

CHAPTER 2

THE DISTANCE MEASUREMENT SYSTEM
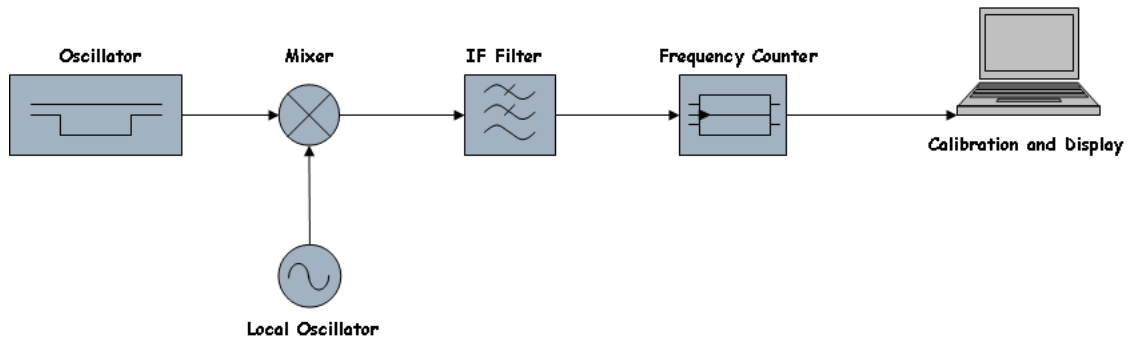
Figure 2.1. The distance measurement system

As seen in Figure 2.1, the distance measurement system consist of six parts: an oscillator, a mixer, a local oscillator, a filter, a frequency counter and a computer, respectively. The resonator gives an output at various frequencies according to the distance between resonator plates that is to be measured. Combination of the mixer, local oscillator, filter and frequency counter provides heterodyne detection. Hereby, the computer is for calibration and to display the results.

2.1. Types of Oscillators for the Measurement System

For the distance measurement system, a microwave sensor is connected to the heterodyne receiver. This microwave sensor is an oscillator whose resonant frequency is changed depending on its movable part. Furthermore, resonators that can be used for distance measurement should be active since the heterodyne system only measures the frequency of an oscillator and do not generate any signal to excite the oscillator. Otherwise a signal generator is needed to excite the resonator. Some oscillators which are appropriate for distance measurements are *Cylindrical Resonator*, *Fabry-Perot Resonator* and *Groove Guide Oscillator*.

Cylindrical Resonator

As depicted in Figure 2.2 which is given in (Bechteler 2004), the Cylindrical Resonator is a cylindrical shaped circular waveguide resonator. In this resonator there exist a piston with a short-circuit slide whose movement changes the frequency of resonance. According to the the distance l, the resonant frequency is changed. For instance, when l is increased, resonant frequency is decreased and vice versa. Since the piston that moves inside the cylindrical waveguide is short-circuited, the relation between the distance l and wavelength λ is

$$l = n\lambda_0/2 \qquad \text{for } TE_{01} \text{ mode} \tag{2.1}$$

In addition, excitation of the cylindrical resonator is done by a coupled rectangular wave guide.
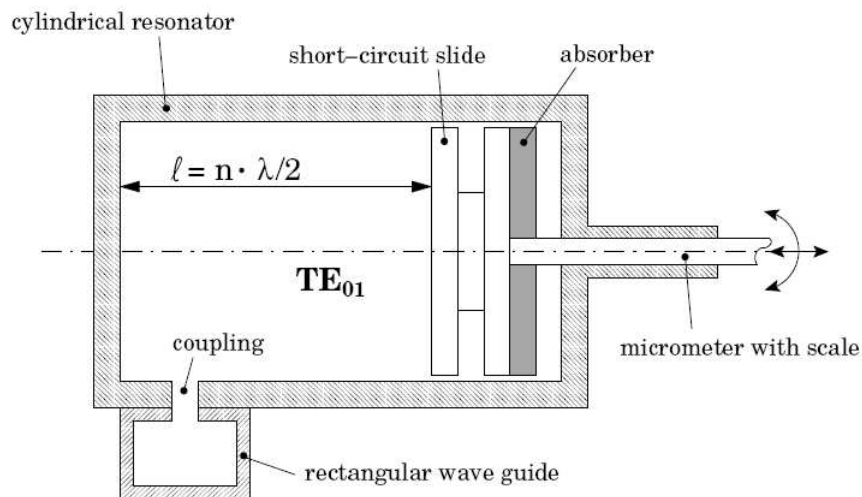
Figure 2.2. Cylindrical resonator

Fabry-Perot Resonator

A Fabry-Perot Resonator consists of two metallic mirrors composed of copper, gold-plated brass or superconductors. It can be seen from the Figure 2.3 that the concave mirror is fixed and the plane mirror is movable. According to the distance D between the plates, the resonant frequency is changed. When D is increased frequency of resonance is decreased and vice versa. Equation (2.2) shows the relation between the distance D and

resonant frequency f_q for the fundamental $TEM_{0,0,q}$ mode, as presented for instance in (Komiyama, et al. 1991).

$$f_q = \frac{c}{2D}\left[q + 1 + \frac{1}{\pi}tan^{-1}\left(\frac{D}{R_0 - D}\right)^{1/2}\right] \tag{2.2}$$

Furthermore, both metallic plates of the resonator can be concave mirrors. However, for the movable plate being a plane mirror makes the system appropriate for distance measurements.
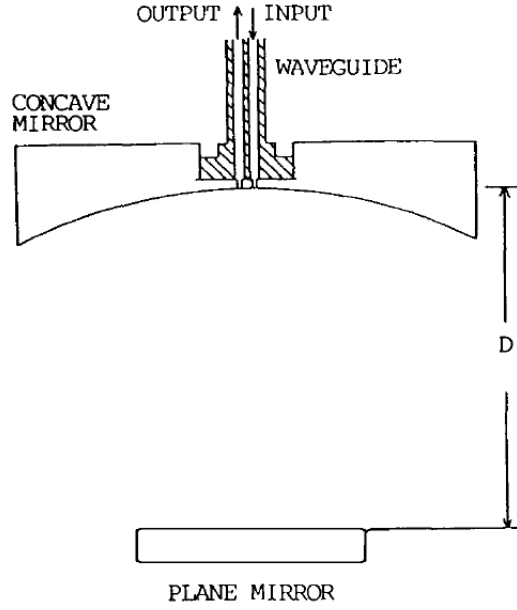
Figure 2.3. Fabry-Perot Resonator

Circular Groove Guide Oscillator

Circular groove guide oscillator consists of a groove guide resonator, which is similar to a ring resonator and an active device. As seen in Figure 2.4, it has a circular groove inside where resonance occurs, and a movable upper plate to change the resonant frequency depending on distance d. For instance, when d is increased the resonant frequency is decreased and vice versa. The resonant frequency f_n of the oscillator is determined by the Equation (2.3) in (Bechteler and Sevgi 2004) where distance $d = 0$ for the dominant TE_{10} mode. It can be seen from the Figure 2.5 that, when $d = 0$, the circular groove guide resonator becomes a simple ring resonator.
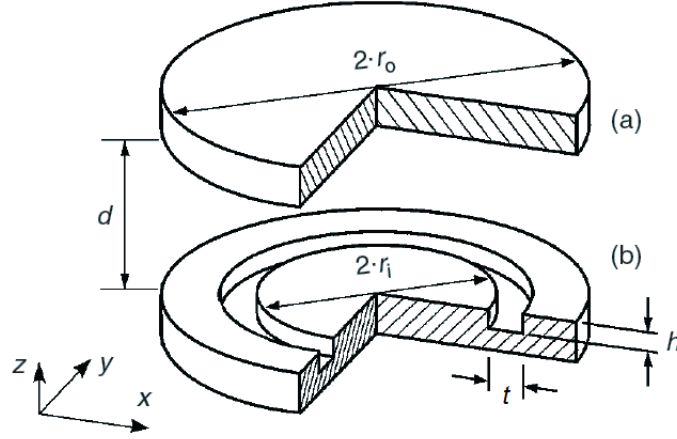
Figure 2.4. Circular groove guide oscillator

$$f_n = \frac{c}{2\pi}\sqrt{\left(\frac{n}{\rho_0}\right)^2 + \left(\frac{\pi}{h}\right)}, \qquad \rho_0 = \frac{a+b}{2} \tag{2.3}$$

where a and b is shown in Figure 2.5.

And as for $d > 0$, there are some analytical approximate formulations named transverse-resonance approach and the improved transverse-resonance approach to obtain a dispersion diagram $\beta = \beta(f)$ (from the cross-sectional resonances) for the groove guide. Thus, Equation (2.4) shows the resonant frequency of the circular oscillator where $d > 0$.

$$(2r_i + t)\pi = n\lambda_g = n\frac{2\pi}{\beta} \tag{2.4}$$

Here, r_i and t are the inner radius of the resonator and the width of the groove, respectively. Also, the effective wavelength in the groove guide is λ_g, and β is the propagation constant. Since the resonator is of circular shape, the integer n describes the periodicity of the structure.

Since groove guide oscillator is an open structure, the oscillator has many advantages such as low-loss and higher powerhandling capacity. Furthermore, it is very easy to excite the oscillator (Bechteler, et al. 2008).
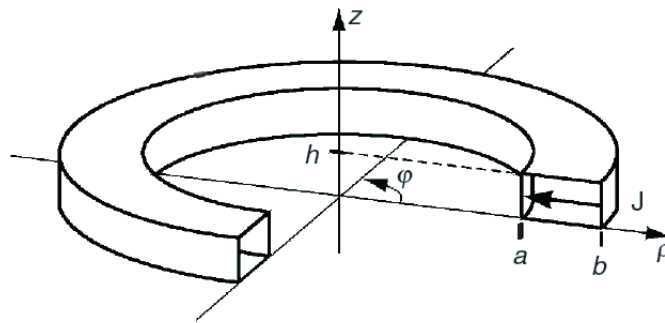
Figure 2.5. The circular groove guide resonator behaves like a ring resonator
when $d = 0$

2.2. Heterodyne Receiver

The heterodyne receiver, sometimes called superheterodyne receiver, is used everywhere in personal communication devices, wireless receivers, LNBs, radar systems, radio astronomy telescopes to radio and TV tuners. The invention of the heterodyne receiver dates back to the early part of 1918. Since, in those years no practical short wave amplifiers existed, in order to amplify short wave signals (at that time any frequency above 500 kHz) for experimental radar applications and long distance reception from broadcasting stations, a heterodyne system depicted in Figure 2.6 was used (Godara 1999). It transforms all incoming signals to an intermediate frequency (IF) where the signals are amplified using tuned amplifiers. Therefore, it is not necesssary to build a tunable high Q filter. Typical heterodyne receiver consists of an RF section, mixer, local oscillator, IF amplifier, detector, power amplifier, and a loudspeaker. The RF section, tuned to the carrier frequency of the wanted signal, receives the signal from the antenna. It has a bandpass filter characteristic in order to suppress image and intermediate frequency signals. Then it performs an amplification. The RF signal, which is the output of the RF section, is multiplied with the local oscillator signal via a mixer to change the carrier frequency to the fixed intermediate frequency. The typical IF frequencies of AM and FM receivers are 0.455 MHz and 10.7 MHz, respectively. Then, the IF section amplifies the IF signal by using tuned amplifiers with the bandwidth of around 10 kHz for AM and around 200 kHz for FM receivers. Furthermore, the output of the IF section is connected to a detector in order to recover the baseband signal. At the end, the signal is amplified again and

delivered to a loudspeaker.
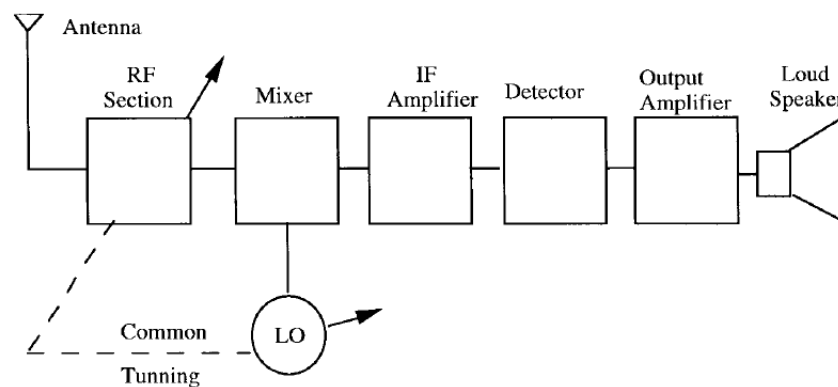
Figure 2.6. Block diagram of a heterodyne receiver

For this thesis heterodyne receiver is set up to measure the groove guide oscillator frequency precisely. In order to do this, as illustrated in Figure 2.7, the system used in this thesis is slightly different from previously mentioned heterodyne receiver and described in Chapter 3. Instead of the classical audio amplifier and a loudspeaker a frequency counter evaluates the signal.
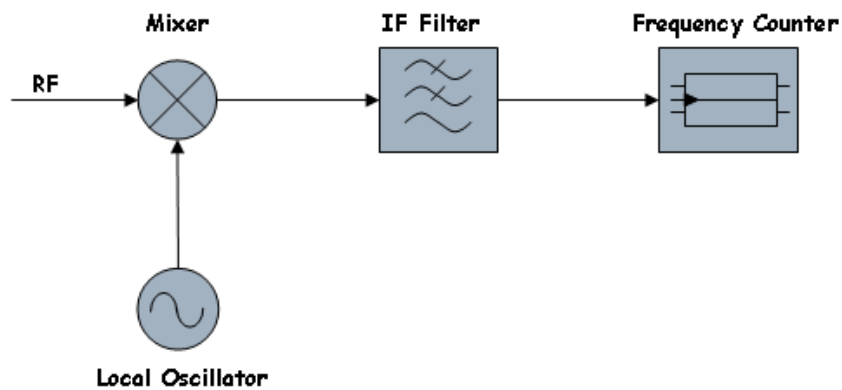
Figure 2.7. Block diagram of a modified heterodyne receiver

CHAPTER 3

PRINCIPLE OF HETERODYNE SYSTEMS

It can be seen from Figure 2.7 that the heterodyne system is modified in order to meet the requirements of the measurement system. In this system the combination of a mixer, a local oscillator, an IF filter, and a frequency counter is used to measure the grooveguide oscillator frequency precisely. The mixer is used to perform the down-conversion process. For instance, if the RF signal is at 10 GHz, and the local oscillator produces a frequency of 12 GHz, by mixing both signals via a mixer, a difference of 2 GHz is obtained (12 - 10 = 2 GHz). This is the intermediate frequency.

The main objective of the superheterodyne receiver is to produce a constant intermediate frequency smaller than the frequencies of the RF signal and the local oscillator. Since, here the aim of the receiver is to measure the various frequency outputs of the grooveguide oscillator that dependents on the distance between the plates, a constant intermediate frequency can not be used. Therefore, a system with a variable intermediate frequency is set up. As the selected output frequency spectrum of the groove guide resonator is between 10 GHz to 12 GHz, a local oscillator with the frequency of 12 GHz is needed. Therefore, the intermediate frequency would be between DC to 2 GHz. However, in order to use the heterodyne system for different oscillators and to increase the distance measurement scale the intermediate frequency from DC to 2.5 GHz is preferred. Thus, the IF filter would be a low-pass filter with the cut-off frequency of 2.5 GHz. Frequency counters operating in this frequency range are cheap. Furthermore, to adapt the receiver for different oscillators, a voltage controlled oscillator (VCO) is used as a local oscillator. In the following sections, the devices used in the receiver are described.

3.1. Voltage-Controlled Oscillator

Oscillators generate a reference signal at a particular frequency. Oscillators are generally used in RF circuits to generate the local oscillator (LO) signal for mixers. Voltage controlled oscillators are used in both receivers and transmitters. In voltage controlled oscillators (VCOs) the frequency of the output varies in proportion to a DC control signal.

As seen in Figure 3.1, V_T is the tuning voltage that controls the output frequency f_{out} and whereas V_{DC} is the supply voltage.
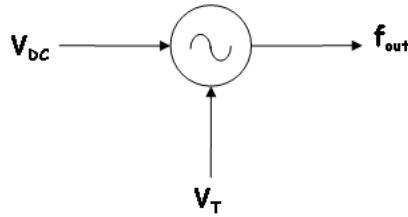
Figure 3.1. Block diagram of a VCO

Generally, a piezoelectric crystal such as quartz is used in oscillators as a resonator. Piezoelectricity is the most significant property of a crystal that makes it usable as a resonator. Piezo is derived from the Greek word *piezin* and means *to press*. Piezoelectricity is an electric polarization produced by mechanical stress in crystals and that polarization is proportional to the stress and the changing sign of the force. This electric polarization provides a source of voltage. Also, the inverse effect can be occured as a voltage applied across the crystal and that produces mechanical movement. The electric polarization can be produced by mechanical stress such as bending, shear, torsion, tension, and compression on a piece of quartz.

A simplified basic oscillator circuit is illustrated in Figure 3.2 with the elements of a quartz crystal, a tunable capacitor, a resistor, and an amplifier (Hewlett-Packard 1997). Quartz crystal is used as a resonator and tunable capacitor provides frequency tuning. When crystal is connected into the amplifier circuit, a small amount of energy is fed back to the crystal and this causes the crystal to vibrate. These vibrations stabilize the generated frequency at the resonant value. Since, capacitance of a varactor diode is changed depending on a voltage, in order to do a voltage controlled oscillator a varactor diode is generally used as a tunable capacitor. The varactor diode is a nonlinear device which provides a voltage dependent capacitance and such kind of diodes operate in reverse bias condition.

However, at high frequencies quartz is generally not used. In this frequency range other technologies such as Gunn diode oscillators or dielectric resonator oscillators are used.

In this study a commercially available voltage controlled oscillator, whose output

frequency spectrum is 11 - 12 GHz, is used.

Feedback
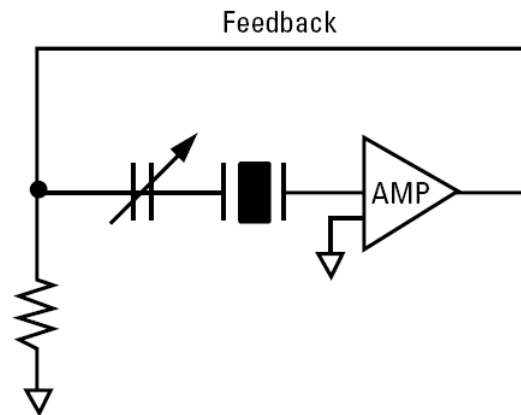
Figure 3.2. A simplified basic VCO circuit

3.2. Mixer

To mix signals into different frequency bands, a nonlinear device is necessary such as diodes and transistors. As a difference, transistor mixer can have a conversion gain since they combine mixing and amplification. Figure 3.3 shows the block diagram of a mixer with its input and output signals. Depending on if the output frequency f_{IF} is higher or lower than the input frequency f_{RF}, the mixer is called up-converter or down-converter, respectively.

local oscillator
f_{LO}

f_{RF}

input RF
signal

f_{IF}

intermediate
signal
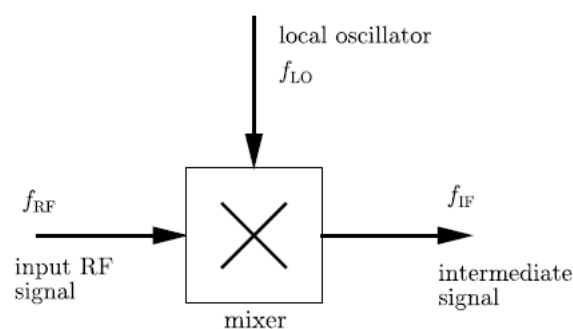
mixer

Figure 3.3. Mixer

In high frequency mixing applications diodes are preferred, because they require simpler bias circuits and they can be used up to very high frequencies ($\approx$ 1000 GHz). Especially Schottky-diodes are used at microwave frequencies. The switching speed of

a diode is a function of the recombination time of minority carriers. With the metal-semiconductor junction, the majority carriers determine the current mechanism. Therefore, Schottky-diodes whose junction is a metal-semiconductor can switch quickly.

The ideal mixer multiplies two input signals of different frequencies. The output signal frequency f_{out} is the sum and the difference of the two input signal frequencies. In general, only one output frequency is wanted, and the other frequency is suppressed by filtering. Ideally, the output level is directly proportional to the signal input level where the signal level of the local oscillator is constant. Furthermore, the phase difference between two input signals remains, when they are mixed with the same local oscillator.

The output spectrum of mixing contains upconverted and downconverted frequency components. Generally, the upconversion is used in generators and the downconversion is used in receivers. Figure 3.4 and Figure 3.5 show the upconversion and downconversion process of mixing where the input frequencies are f_s as the signal frequency and f_{LO} as the local oscillator.

Figure 3.4. Frequency representation of upconversion
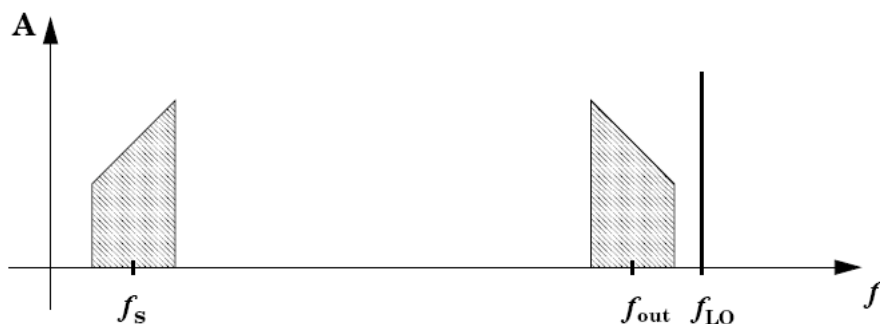
Figure 3.5. Frequency representation of downconversion

13

In reality, there is no ideal mixer. Therefore, aside from the sum and difference of the input signals also harmonics appear. Furthermore, the output signal contains the input signal frequencies. The output frequencies due to intermodulation are given as

$$f_{out} = |m f_s \pm n f_{LO}|,$$ (3.1)

where m, n = 0, 1, 2, ... For instance, if $m = 0$, $n = 1$ or $n = 0$, $m = 1$ the output signal frequency is f_{LO} or the input signal f_s, respectively. For the case $m = n = 1$, the output signal frequency is called product of second order. Furthermore, If $m = n = 2$, the output signal frequency is called product of fourth order. And other high order products are occured as $m = n = 3, 4, 5, \ldots$

A commercially available double-balanced downconversion mixer is used in order to meet the heterodyne receiver requirements, since for heterodyning downconversion process is necessary.

Double-Balanced Mixer

The double-balanced mixer can be constructed in several ways (Pavio, et al. 1988, Henderson 1990). One of the most common design is the ring modulator depicted in Figure 3.6.
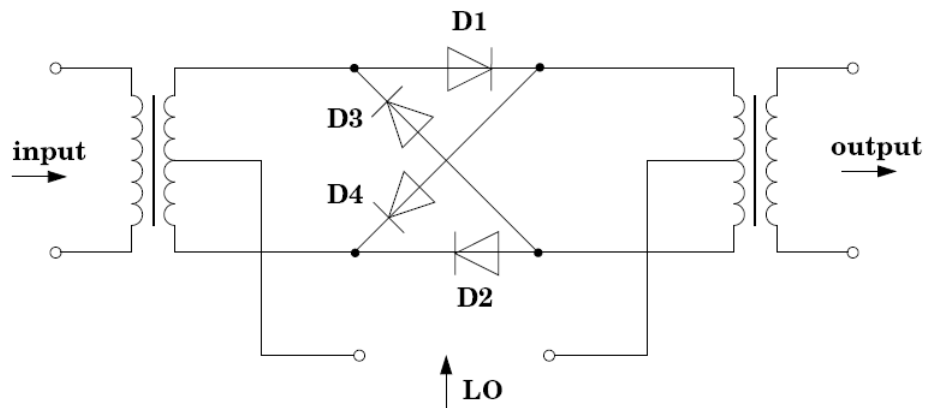
Figure 3.6. A schematic of a double-balanced mixer

By considering the diodes as switches, it is easy to understand the functionality of this mixer. By a positive LO signal the diodes D1 and D2 are switched on and the diodes D3 and D4 are switched off. By a negative LO signal the diodes are switched vice versa.

Thus, the polarity of the input signal is changed by the clock of the LO signal. In other words, the output signal is the multiplication of input signal with a square-wave signal. Due to the spectrum of the square-wave signal, the frequencies of the output signal can be determined by Equation (3.1) where $m = 1$ and $n = 1, 3, 5, \ldots$ Here, the case $m = 0$ or $n = 0$ do not exist. That means the input signal frequency and the LO signal frequency can not be seen as the output frequency. In the real ring-mixer the diodes are not being switched by a square-wave signal but a sinusoidal signal. However, the input and LO signals are sufficiently decoupled from the output due to fast switching diodes.

3.3. Frequency Counter

The frequency measurement is one of the fundamental issues in experimental studies. The time t is related with the frequency f via the period T by the well-known equation $f = 1/T$. Furthermore, a transform from frequency to wavelength is possible by the equation $c = \lambda f$ and vice versa. In mechanical frequency meters the frequency is determined by a length measurement. This length measurement is done by a fraction or a multiple of the wavelength of the signal. Mechanical frequency meters are the Standing Wave Detector, Michelson Interferometer and Resonant Frequency Meter. The principle of the measurement for Standing Wave Detector and Michelson Interferometer is based on detection of interference patterns. As for Resonant Frequency Meters, measurement is done by measuring the resonant frequency of a resonator. However, for the lower frequency range these measurement methods are not convenient because of the mechanical size of such systems.

Electronical frequency counters measure the frequency directly and can operate up to 500 MHz. For higher frequency measurements, dividers (nowadays up to 4 GHz) can be used. For even higher frequencies a mixer is necessary to convert the high frequency down to a measurable frequency (Intermediate frequency) and this is the main reason heterodyne receiver is used in this study.

To measure the frequency of the intermediate frequency (DC to 2.5 GHz), a commercially available Tecstar FC-2500 is used for this application.

3.4. IF Filter

In order to suppress any frequency apart from intermediate frequency, a filter is necessary. Since the intermediate frequency is from DC to 2.5 GHz, a low-pass filter with the cut-off frequency of 2.5 GHz is needed. As for the type of the filter, a Chebyshev low-pass filter is prefered due to the steepest slope at the stopband region. Thus, a 3rd order Chebyshev low-pass filter with the cut-off frequency of 2.5 GHz and passband ripple of 0.5 dB is designed and described in the next chapter.

Low-pass filters are commonly used in various electronic devices to suppress unwanted signals or interference from surrounding enviroment. For instance, low-pass filters are used in radio transmitters to block harmonic emissions that may cause interference with other communications. In audio systems, a sub-woofer will use a low-pass filter to remove the higher frequencies. Many techniques can be used to implement different type of filters like passive lumped elements, active lumped elements, waveguides, microstrip lines. At lower frequencies lumped element inductors and capacitors are used to design filters. However, at microwave frequencies generally transmission line sections or waveguide elements are used. In mobile communication devices a different type of filter that is named surface acoustic wave (SAW) is used. In SAW filters a piezoelectric material oparates to create surface acoustic waves that provides the filter characteristic.

Beyond 500 MHz, filter designs are difficult to realize with lumped elements since the wavelength becomes comparable with the physical dimensions of filter elements and distance between them. This case causes various losses and degrades the circuit performance. Therefore, for this thesis a microstrip line low-pass filter is designed and realized.

Microstrip Lines

As illustrated in Figure 3.7 given in (Bechteler 2004), microstrip lines consist of a conductor of width w printed on a dielectric substrate of thickness h and permittivity ε. Buttom side of the dielectric substrate is covered by a grounded conductor. In a microstrip transmission line the dielectric substrate does not completely surround the conducting strip. Therefore, the fundamental mode of propagation is not a pure TEM mode. It can be seen from the Figure 3.8 that most of the field lines are kept in the dielectric region and some of them are in the air region. Electric and magnetic fields are propagating in z-

direction. At the boundary between air and the dielectric medium the normal components of the electric field are not equal. The phase velocity equals to c in the air region and $c/\sqrt{\varepsilon_r}$ inside the dielectric region. Thus, a TEM-type wave can not be propagate due to the impossibility of a phase match at the dielectric-air interface.
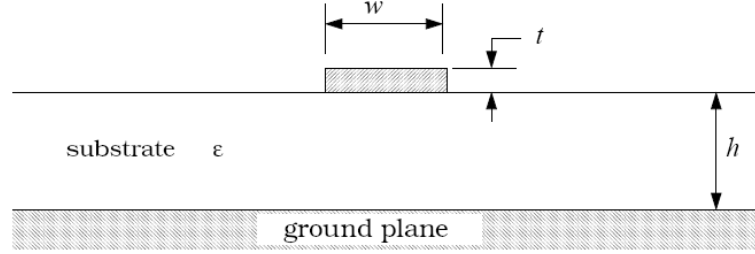
Figure 3.7. Microstrip line in cross-sectional view
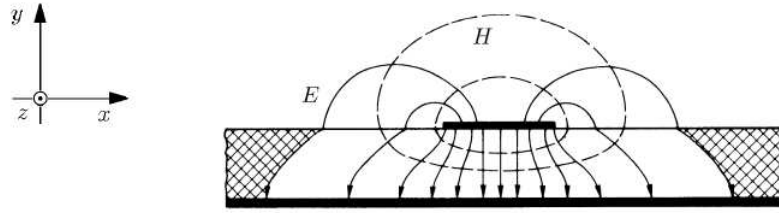
Figure 3.8. E and H field on a microstrip line

The design equations for the characteristic parameters of microstrip lines are given below and represented in (Hammerstad 1975, Hammerstad and Jensen 1980).

$$Z_{msl} = \begin{cases} \dfrac{\sqrt{\mu_0/\varepsilon_0}}{2\pi\sqrt{\varepsilon_{r,eff}}} ln\left(\frac{8h}{w} + 0.25\frac{w}{h}\right) & \text{for } w/h \leq 1 \\[4mm] \dfrac{\sqrt{\mu_0/\varepsilon_0}}{\sqrt{\varepsilon_{r,eff}}}\left[\frac{w}{h} + 1.393 + 0.667 \times ln\left(\frac{w}{h} + 1.444\right)\right]^{-1} & \text{for } w/h > 1 \end{cases} \tag{3.2}$$

$$\varepsilon_{r,eff} = \frac{\varepsilon_r + 1}{2} + \frac{\varepsilon_r - 1}{2} \times func(w/h) \tag{3.3}$$

with:

$$func(w/h) = \begin{cases} \dfrac{1}{\sqrt{1 + 12h/w}} + 0.04\left(1 - w/h\right)^2 & \text{for } w/h \leq 1 \\[4mm] \dfrac{1}{\sqrt{1 + 12h/w}} & \text{for } w/h > 1 \end{cases}$$

In Equation (3.2) and Equation (3.3) the thickness t of the MSL is not included. However, this parameter has nearly no infuence on the accuracy of these equations. Especially, the thickness t is important for the losses. If microstrip lines are compared with coaxial lines and waveguides their losses are very high. It can be seen from the Equation (3.3) that in order to use MSLs at as high as possible frequencies, the height h of the substrate must be small. Thus, microstrip lines are used up to 20 GHz.

CHAPTER 4

THEORY, DESIGN and TESTS of the HETERODYNE SYSTEM

In order to determine optimum operating conditions and the limitations of devices, some tests are performed. Therefore, this chapter provides characterisations of the parts of the heterodyne system, such as VCO, mixer and frequency counter. Furthermore, a microstrip line low-pass Chebyshev filter is designed, realized and tested. Finally, the conversion of gathered datas, eg. frequency to distance, is also described in section 5.

4.1. VCO Characterisation

To achieve optimal circuit performance, VCO characteristics or parameters under varying conditions should be measured and discussed. As an example, one fundamental parameter is the plot of the VCO output frequency versus the tuning voltage. An extension of this parameter is tuning sensitivity (expressed in Hz/V), which is the differential of the output frequency versus tuning voltage curve.

In practice, both of these parameters should be evaluated under different supply (V_{DC}) conditions since the output frequency may shift with V_{DC} changes. This DC power sensitivity is called frequency pushing. The RF power output is also a function of both V_{DC} and output frequency. The output power of a VCO is typically expressed in dBm. The parameters that are covered in this section are listed and described in the following subsections.

As mentioned in the previous chapter, a commercially available voltage-controlled oscillator illustrated in Figure 4.1, is used as the device under test. A spectrum analyzer with the frequency range 30 Hz to 50 GHz is used in order to measure the output frequency and the output power of the VCO. Also, well regulated power supplies are recommended for tuning and VCO supplies.
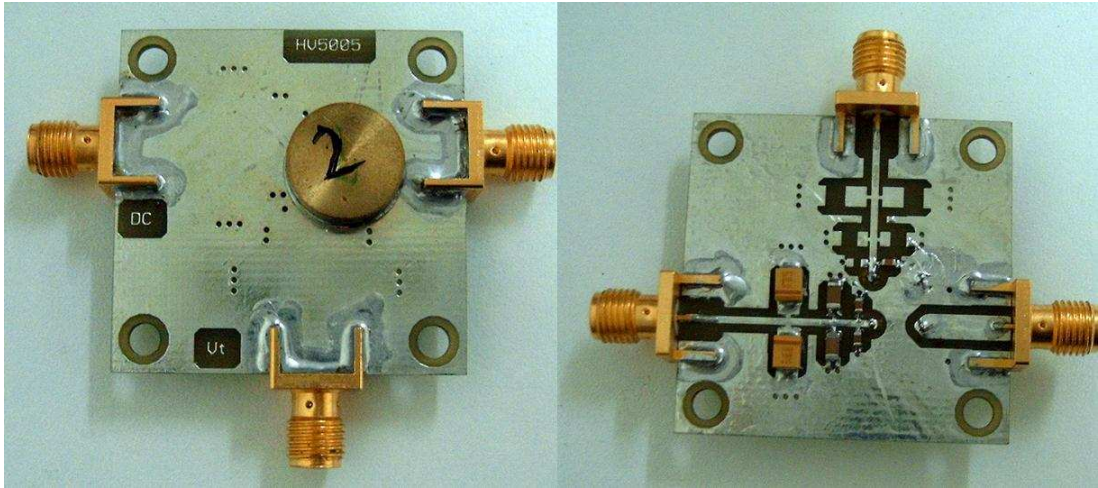
Figure 4.1. Top and buttom view of the commercially available VCO

4.1.1. Effect of the Supply Voltage

The frequency of a voltage-controlled oscillator is varied by tuning voltage value (V_t). Unfortunately, the supply voltage may also influence the frequency of the VCO. Therefore, the supply voltage is varied to see the effect on the output spectrum of the VCO. Figure 4.2 illustrates the block diagram of the setup for this measurement.
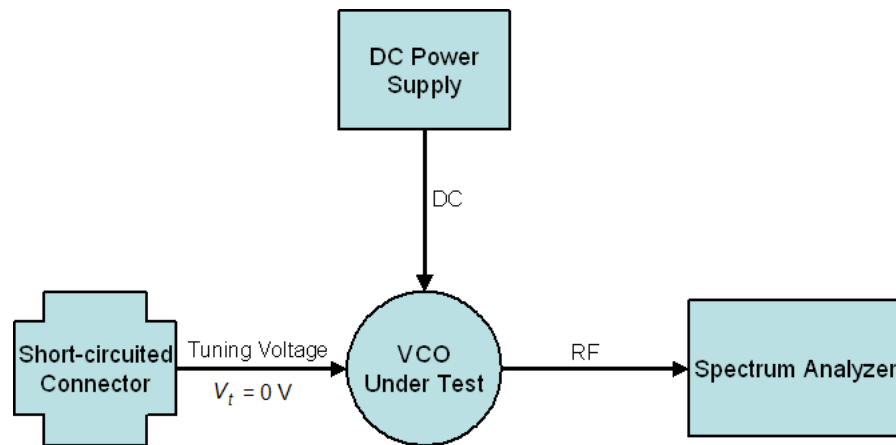
Figure 4.2. Supply voltage test setup

V_t input port is short circuited to set the port at 0 V (GND) in order to provide the frequency output change because of V_{DC}. According to the datasheet of the VCO, typical DC Voltage value is 5 V and typical DC current value is 0.06 A. Therefore, V_{DC} is increased from 4 V to 5 V in 0.1 V steps via a DC power supply. Thus, supply current,

output spectrum and power difference between the first and the second harmonics are observed for each V_{DC} value while V_t is 0 V. Measurement results are listed in Table 4.1 and Table 4.2, and plotted in Figure 4.3 through Figure 4.5. In the tables shown below, V_{DC} is the supply DC voltage of the VCO, f_{out} is the output frequency, P_{out} is the output power in dBm, I_{DC} is the supply current and (P_Δ) is the power difference between the first and the second harmonic.

Table 4.1. Supply voltage analysis

V_{DC} [V]	f_{out} [GHz]	P_{out} [dBm]	I_{DC} [A]
4	11.878	-1.83	0.04
4.2	11.884	0.5	0.04
4.4	11.891	2.67	0.05
4.5	11.894	3.83	0.06
4.6	11.8951	4.5	0.06
4.7	11.8958	5	0.07
4.8	11.8954	5.33	0.07
4.9	11.8933	5.67	0.08
5	11.8898	5.83	0.09

Table 4.1 shows that supply current satisfies 0.06 A only when V_{DC} is 4.5 V and 4.6 V and at that rates output frequencies are 11.894 GHz and 11.8951 GHz. Also, it can be seen from Table 4.2 that power difference between the first and the second harmonic (P_Δ) is about 25 dB and increases as V_{DC} increases.

In order to use the VCO at optimum operating conditions, supply power should be lower and power difference between the first and the second harmonic should higher. Additionally, the effect of supply voltage on the output frequency should be taken into consideration according to wanted output frequency while V_t is 0 V. Thus, when measurement results shown in Figure 4.3 through Figure 4.5 and criterions are taken into account, V_{DC} is determined to be 4.5 V. Most important, the DC power supply that feeds the V_{DC} port of the VCO must be stable otherwise the output frequency will be affected by V_{DC} aside from V_t.

Table 4.2. Power difference between the 1st and the 2nd harmonics

V_{DC} [V]	P_Δ [dB]
4	23.33
4.2	23.83
4.4	24.66
4.5	25.34
4.6	25.5
4.7	26.33
4.8	26.66
4.9	27
5	27.17
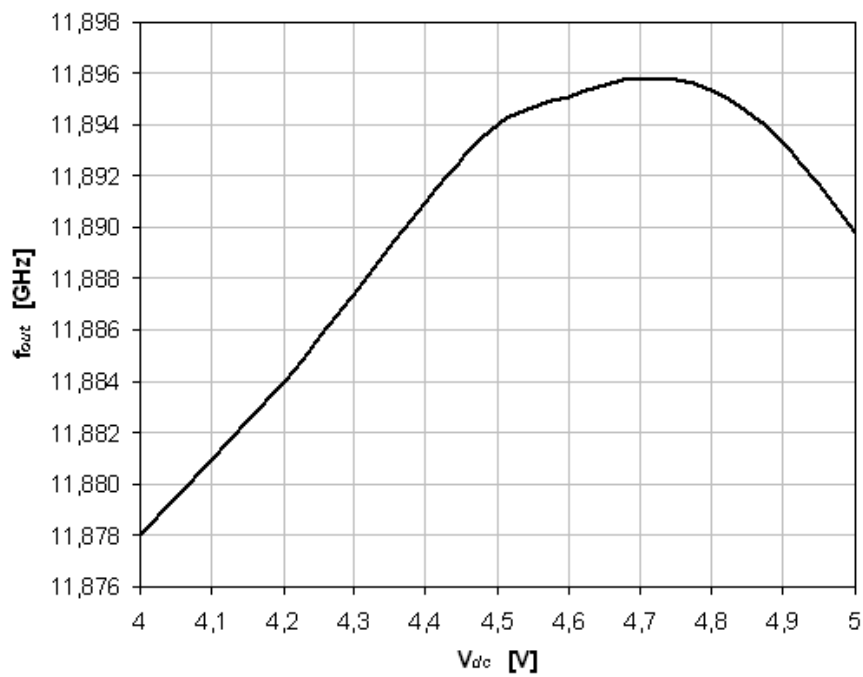
Figure 4.3. Output frequency versus supply voltage
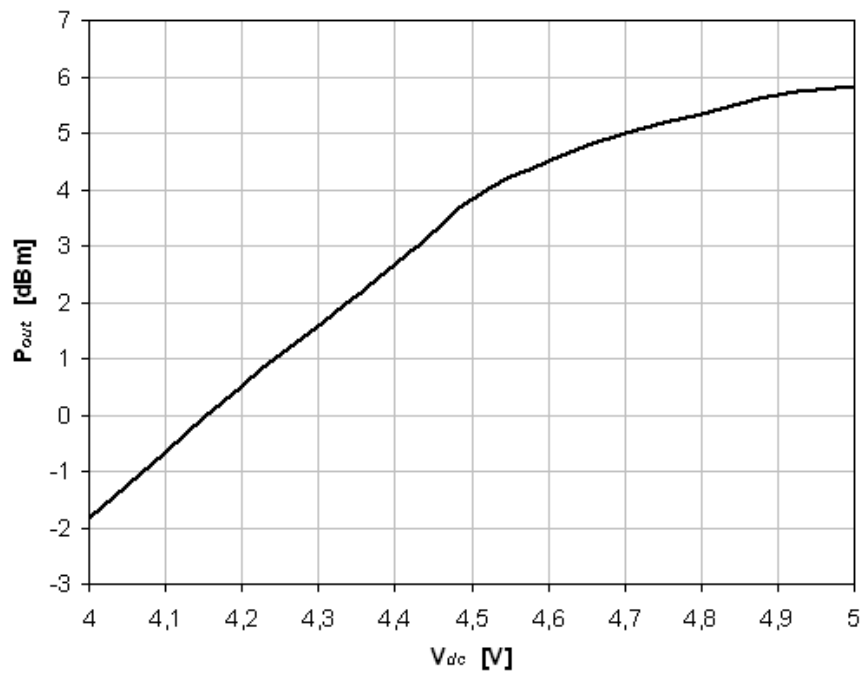
Figure 4.4. Output power versus supply voltage
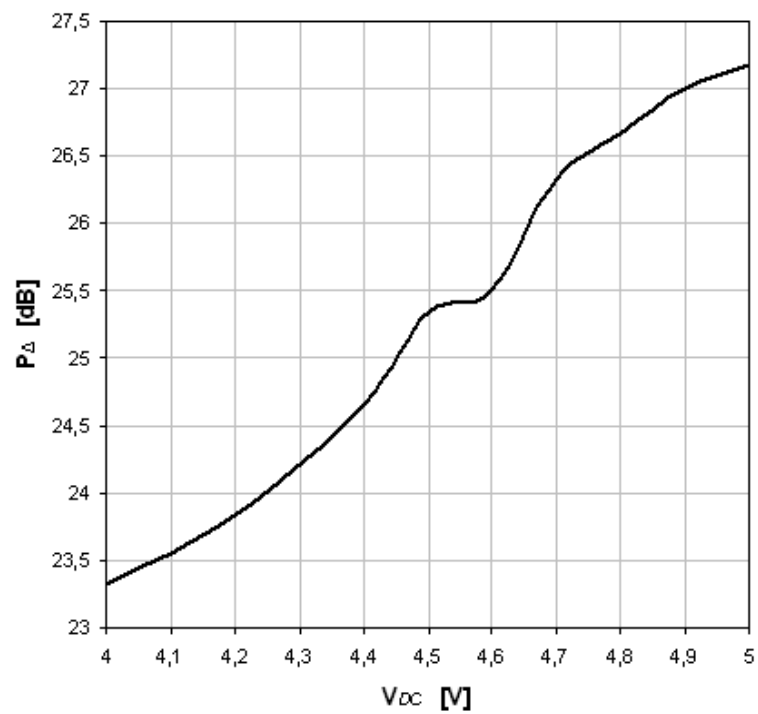
Figure 4.5. Power difference between the 1st and the 2nd harmonics

4.1.2. Output Frequency and Output Power According to Tuning Voltage

For a constant voltage of 4.5 V, the output frequency of the VCO according to the tuning voltage is measured. This characteristic is significant since V_t determines the output frequency and output power of a VCO. Figure 4.6 depicts the block diagram of the setup for this measurement.
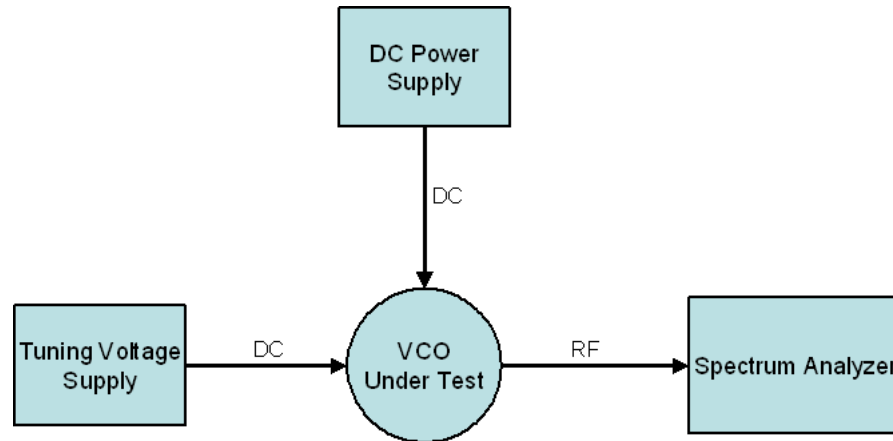
Figure 4.6. Output frequency and output power tests setup

V_{DC} is set to 4.5 V, and both the output frequency and output power are measured while V_t is changed from 0 V to 5 V in 0.5 V steps. Measurement results are presented in Table 4.3.

As seen in Table 4.3, output frequency of the VCO is varying from 11.896 GHz to 12.196 GHz and increases as V_t increases. As for the output power, it is between 3.50 dBm and 0.67 dBm and decreases as V_t increases. The results of the measurements are shown in Figure 4.7 and Figure 4.8.

Tuning sensitivity is defined as the frequency change per unit of tuning voltage. Ideally, the tuning sensitivity should be constant but in practice it may not be constant. Measure the VCO frequency for different tuning voltages and plot VCO frequency measurements against tuning voltage. The slope of this characteristic is the tuning voltage sensitivity which you can calculate at different tuning voltages. The tuning sensitivity is expressed in Hz/V.

Amount of frequency change (Δf) due to tuning voltage is illustrated in Table 4.4. It can be seen from Figure 4.7 that the VCO exhibits a nearly linear output frequency char-

Table 4.3. Output frequency and output power according to tuning voltage

V_t [V]	f_{out} [GHz]	P_{out} [dBm]
0	11.896	3.50
0.5	11.908	3.50
1	11.940	3.17
1.5	11.967	2.67
2	11.993	2.33
2.5	12.025	2.17
3	12.063	1.83
3.5	12.095	1
4	12.127	1
4.5	12.159	1
5	12.196	0.67
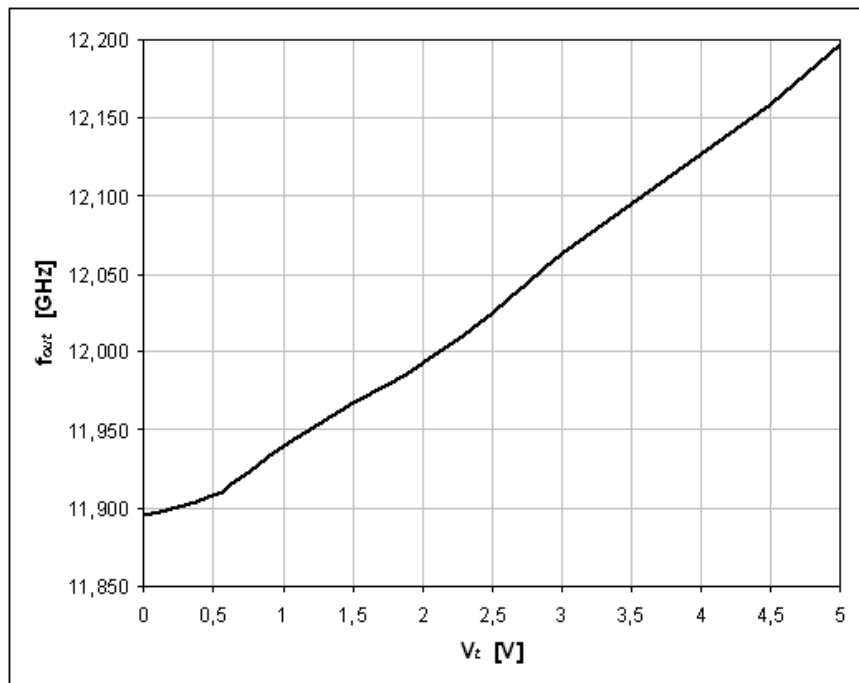
Figure 4.7. Output frequency versus tuning voltage
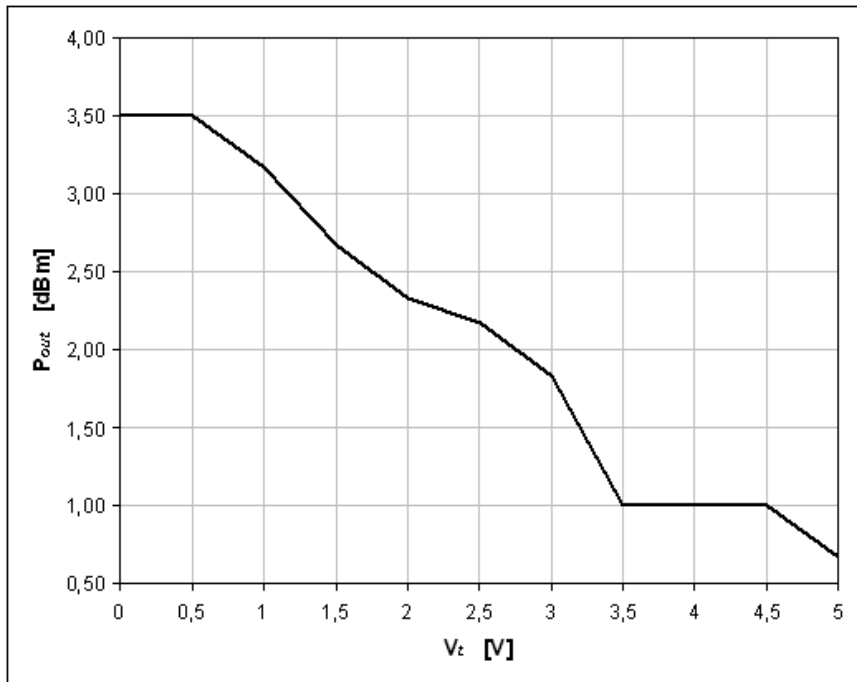
Figure 4.8. Output power versus tuning voltage

Table 4.4. Amount of frequency change according to tuning voltage

V_t Interval [V]	Δf [MHz]
0 - 0.5	12
0.5 - 1	32
1 - 1.5	27
1.5 - 2	26
2 - 2.5	32
2.5 - 3	38
3 - 3.5	32
3.5 - 4	32
4 - 4.5	32
4.5 - 5	37

acteristic. According to Table 4.4, the average tuning sensitivity of the VCO is calculated to be 60 MHz/V.

4.1.3. Phase Noise Measurement

4.1.3.1. Phase Noise

Phase noise and the noise floor are fundamental properties of signals. In contrast to harmonic signals, noise can not be described by amplitude and frequency.

Phase noise is defined as frequency fluctuations of a signal from a medium frequency. This frequency fluctuations are statistical and of short-time. In many cases the applicability of components, like signal sources, mixers and amplifiers, or a whole system is limited by the phase noise. As seen in Figure 4.9 presented in (Thumm, et al. 1998), the influence of the phase noise on a microwave system can be demonstrated with means of a superheterodyne receiver. Phase noise is the most significant source of noise in oscillators, which makes it a crucial measurement. Due to the phase noise, the spectrum of the local oscillator (LO) is widened, and after the mixing, it is transferred to the input signals. In presence of a strong interfering signal close to a weak desired signal, the widened spectrum of the interfering signal can mask the desired signal. This reduces the selectivity of the system. Stronger desired signals can be detected, however, with a deteriorated signal-to-noise ratio. This reduces the dynamic of the system.
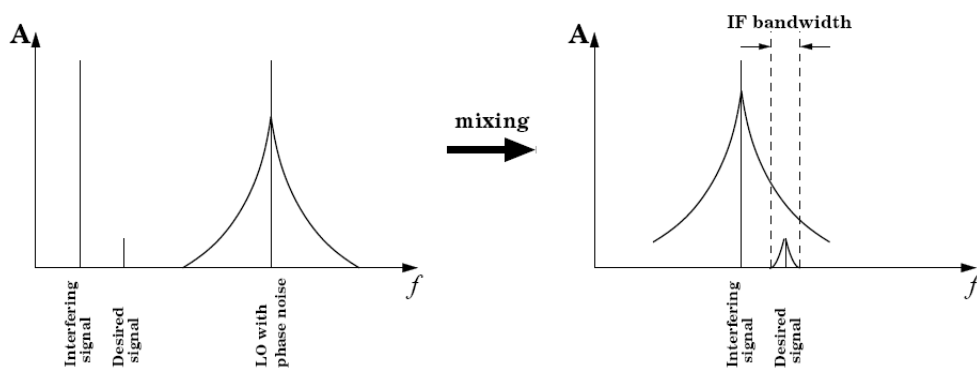
Figure 4.9. Limitation of the selectivity due to phase noise of a VCO

The phase noise is different from the amplitude noise. This can be elucidated by means of the time-function of a monofrequent but noisy signal with the medium frequency

f_m and the medium amplitude U_m.

$$u(t) = [U_m + \varepsilon(t)] \cdot sin[2\pi f_m t + \Delta\phi(t)] \qquad \text{with} \qquad \Delta\phi(t) = 2\pi \int_t \Delta f(t')dt' \quad (4.1)$$

In Equation (4.1) the amplitude fluctuation is described by $\varepsilon(t)$, the phase fluctuation by $\Delta\phi(t)$ and the frequency fluctuation by $\Delta f(t)$. The signal is called carrier, and the noise spectra are given in the spectrum range depending on the offset frequency

$$\delta f = f - f_m\,. \tag{4.2}$$

There are two different kinds of noise definitions, the white noise and the flicker noise. The white noise is due to thermal noise or to shot noise and is frequency-independent ($\sim f^0$). The flicker noise measured in a VCO is generated by active devices, such as the transistor and the tuning diode. The mechanisms for the flicker noise are still under investigation, and it is proportional to the frequency with f^{-1}. Described is the flicker noise by the corner frequency f_c where the noise level of the flicker noise is equal to the level of the white noise. Figure 4.10 shows the flicker noise, the white noise and the corner frequency (f_c).
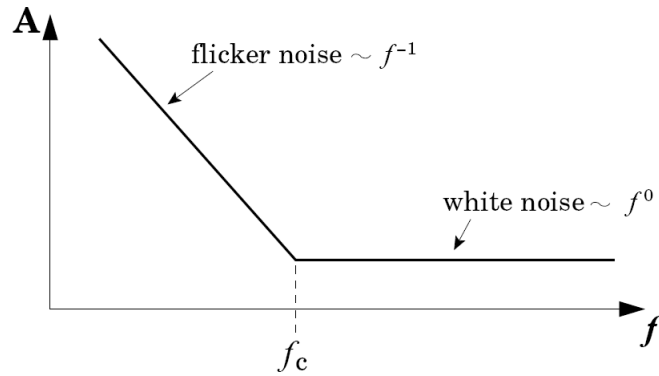
Figure 4.10. Primary noise sources

The effect of the flicker noise takes place when a nonlinear device is used. If a multiplicative superposition occurs, the flicker noise affects the output and causes the phase noise to be transformed into higher frequency bands. On the contrary, for additive superposition the phase noise is not transformed due to the linear superposition. The superposition of the noise with an RF signal of the frequency f_0 is illustrated in Figure 4.11 and Figure 4.12.
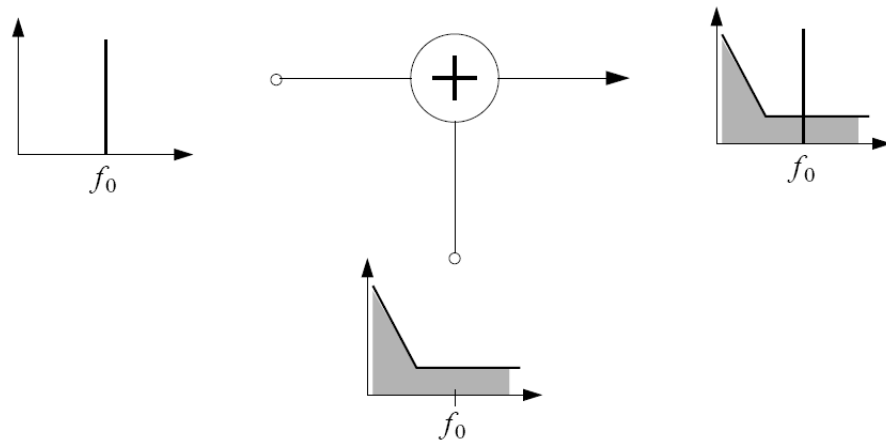
Figure 4.11. Additive (linear) superposition
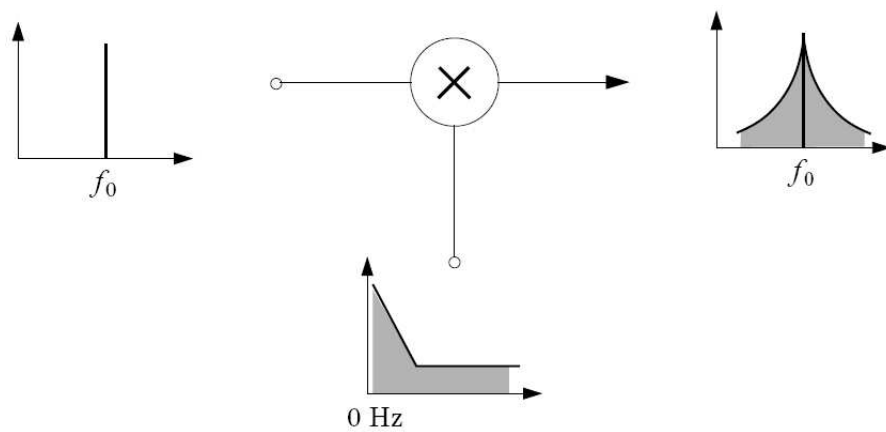
Figure 4.12. Multiplicative (nonlinear) superposition

The single-sideband phase noise is the most used definition to describe the phase noise quantitatively and is defined as the spectral power density of one sideband:

$$S_{SSB}(\delta f) = \frac{\text{Noise Power of one Sideband at } \delta f}{(\text{Measurement Bandwidth}) \cdot (\text{Overall Signal Power})} \tag{4.3}$$

For small phase fluctuations (<0.2 rad) the single-sideband phase noise can be simply expressed as

$$S_{SSB}(\delta f) = \frac{\Delta\phi_{rms}^2}{2B} = \frac{S_\phi(\delta f)}{2} \qquad \text{in [W/Hz]}$$

$$= S_\phi(\delta f) - 3\,\text{dB} \qquad \text{in [dBc/Hz]}. \tag{4.4}$$

In this case, the whole power density is within the sidebands of first order. In general, both sidebands (lower and upper) show the same amplitude. For high phase fluctuations, Equation (4.4) gives incorrect values. The power density of the phase fluctuations at the offset frequency δf is now distributed over several (or many) sidebands of higher order.

In Equation (4.4) the spectral power density of the phase fluctuation ($S_\phi(\delta f)$) is the fundamental description of the phase noise. It is defined as the square of the effective phase fluctuations $\Delta\phi_{rms}^2$ with respect to the measurement bandwidth B:

$$S_\phi(\delta f) = \frac{\Delta\phi_{rms}^2}{B} \qquad \text{in [rad}^2\text{/Hz]} \tag{4.5}$$

This definition is used for describing the effect of the phase noise on phase sensitive systems, e.g. Pulse-Modulation-Communication systems.

Three main methods are used to measure the phase noise. The first method described in the following section involves measuring phase noise directly on a spectrum analyzer. Therefore it is called direct measurement. This measurement can be done as long as the analyzer has lower phase noise than the measured source. In the second method named phase detector method, a better source is phase locked to the same frequency with the 90 phase difference. The mixed product of the unit under test and the reference signal is measured using a FFT analyzer. The idea for this method is to measure the phase fluctuation of a signal with respect to a reference signal. The phase detector method is the most sensitive method to measure the phase noise. It is also called the Two-Oscillator-Technique and used frequently. It is applicable in the same wide frequency range as the

direct method with the spectrum analyzer. The third method uses a discriminator and compares the signal to itself delayed in time and is called the frequency-demodulation-detector method. The spectral power of the frequency fluctuation is measured. This measurement is limited for close-in offsets, because a large part of close-in noise is canceled. The big advantage of this system is that it does not require an excellent reference. In this study the direct method is employed to measure the phase noise level.

4.1.3.2. The Direct Method - Spectrum Analyzer

In case that the phase noise is high, it can be measured simply with a spectrum analyzer. Thus, the singlesideband phase noise is measured directly. The great advantage of this method is its simple measurement setup since the device-under-test is simply connected to the spectrum analyser. The disadvantages are:

- The spectrum analyzer does not distinguish between AM noise and PM noise.

- The measurement sensitivity is limited by the noise of the spectrum analyzer.

- The measurement range to small offset frequencies is limited by the phase noise of internal local oscillators of the spectrum analyser and by the resolution bandwidth of the internal filters of the spectrum analyzer.

- At high phase noise levels, the single-sideband phase noise does not represent the phase noise correctly.

- A frequency drift of the device-under-test disturbs the display, especially at very slow sweep times required for a high frequency resolution.

Data Correction

The displayed level of the spectrum analyzer has to be corrected due to some systematical errors, to obtain the correct value for $S_{SSB}(\delta f)$.

- The displayed value has to be normalised to the common equivalent noise bandwidth of 1 Hz.

- The equivalent noise bandwidth of the resolution bandfilter has to be determined. For Gaussian filters: $B_{noise} = 1.2 \cdot B_{3dB}$. ($B_{noise} = \dfrac{\int_t^\infty \mid H(f) \mid^2 df}{\mid H(f_0) \mid^2}$, with $H(f)$

as the transfer function and wih f_0 as the center frequency of the filter, where the transfer function has its maximum.)

- To obtain the value for $S_{SSB}(\delta f)$ in dBc, the displayed value has to be normalised to the total signal power. For small phase fluctuations ($\Delta\phi_{max} \leqslant 0.2$ rad) the total signal power is represented approximately by the power of the carrier frequency.

- Spectrum analyzers are commonly calibrated for sinusoidal signals. Therefore, the noise level is displayed of about 2.5 dB smaller.

This systematic error of -2.5 dB is caused by two effects. First of all, noise peak-levels are less amlified than middle or low noise levels by a logarithmic amplifier used in spectrum analysers. On the other hand, the level of broadband signals is evaluated very low, because peak-value detectors used in spectrum analysers are calibrated for smallband signals.

VCO is tested as seen in Figure 4.2 in order to measure the phase noise. The offset frequency (δf) is taken 20 kHz, 50 kHz, 100 kHz and 150 kHz respectively. Measurement results which are the power levels of the carrier frequency and various offset frequencies are shown below in Table 4.5, where the resolution bandwidth of the spectrum analyzer is 1 kHz. Here the single-sideband noise level is the sums of the measured power level at δf and the systematic error with the equivalent bandwidth and the power level of carrier.

Table 4.5. Measured power levels of the carrier frequency and various offset frequencies

$P(f_c)$	3.77 dBm
$P(\delta f = 20\,\text{kHz})$	-35.23 dBm
$P(\delta f = 50\,\text{kHz})$	-42.90 dBm
$P(\delta f = 100\,\text{kHz})$	-51.07 dBm
$P(\delta f = 150\,\text{kHz})$	-54.07 dBm

By using the measurements that are shown in Table 4.5 and the data correction procedure mentioned above, phase noise levels are calculated and the results are shown in Table 4.6 through Table 4.9.

Table 4.6. Phase noise calculation where δf = 20 kHz

Measured power level at δf = 20 kHz	$-35.23\,\text{dBm}$
Systematic error	$+2.5\,\text{dB}$
Equivalent noise bandwidth	$-10\log(1.2 \cdot 1\,\text{kHz}) = -30,79\,\text{dB}$
Level of carrier	$-(+3.77\,\text{dBm})$
Single-sideband noise level	$S_{SSB}(20\,\text{kHz}) = -67.29\,\text{dBc/Hz}$

Table 4.7. Phase noise calculation where δf = 50 kHz

Measured power level at δf = 50 kHz	$-42.90\,\text{dBm}$
Systematic error	$+2.5\,\text{dB}$
Equivalent noise bandwidth	$-10\log(1.2 \cdot 1\,\text{kHz}) = -30,79\,\text{dB}$
Level of carrier	$-(+3.77\,\text{dBm})$
Single-sideband noise level	$S_{SSB}(50\,\text{kHz}) = -74.96\,\text{dBc/Hz}$

Table 4.8. Phase noise calculation where δf = 100 kHz

Measured power level at δf = 100 kHz	$-51.07\,\text{dBm}$
Systematic error	$+2.5\,\text{dB}$
Equivalent noise bandwidth	$-10\log(1.2 \cdot 1\,\text{kHz}) = -30,79\,\text{dB}$
Level of carrier	$-(+3.77\,\text{dBm})$
Single-sideband noise level	$S_{SSB}(100\,\text{kHz}) = -83.13\,\text{dBc/Hz}$

Table 4.9. Phase noise calculation where $\delta f = 150$ kHz

Measured power level at $\delta f = 50$ kHz	$-54.07\,\text{dBm}$
Systematic error	$+2.5\,\text{dB}$
Equivalent noise bandwidth	$-10\log(1.2 \cdot 1\,\text{kHz}) = -30,79\,\text{dB}$
Level of carrier	$-(+3.77\,\text{dBm})$
Single-sideband noise level	$S_{SSB}(150\,kHz) = -86.13\,\text{dBc/Hz}$

In Table 4.6 through Table 4.9, the 1 kHz used in the equivalent bandwidth calculation is the adjusted resolution bandwidth (B_{3dB}) of the spectrum analyzer. The phase noise of the VCO is plotted in Figure 4.13.
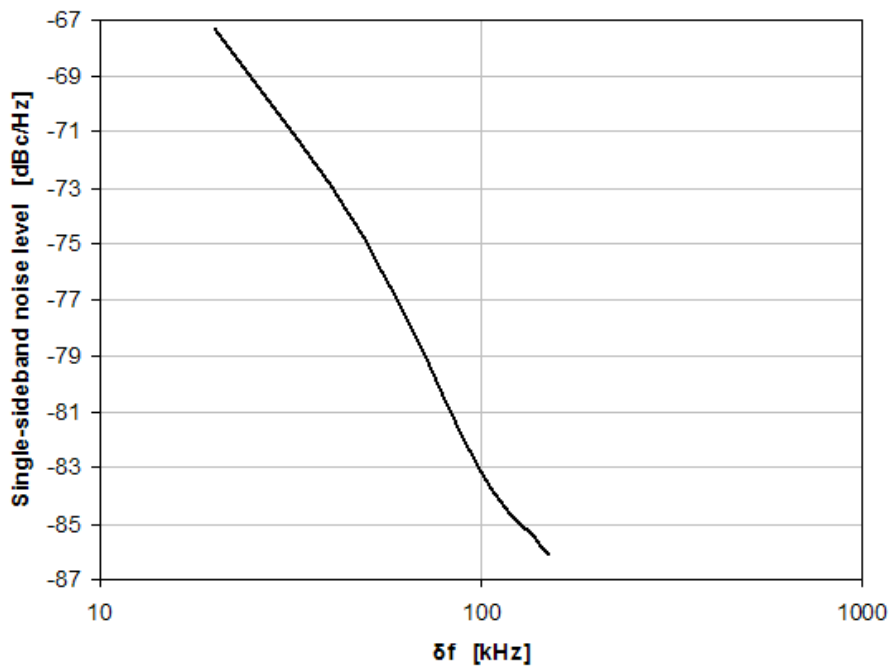
Figure 4.13. Offset frequency versus phase noise

4.1.4. VCO Characterisation Summary

All of the measurement results are summarized in Table 4.10 as several VCO characteristics and parameters.

Table 4.10. VCO Characterisation Summary

Parameter	Minimum	Typical	Maximum	Units
Frequency Range	11.896		12.196	GHz
Phase Noise at 100 kHz		-83.13		dBc/Hz
Tuning Voltage	0		5	V
Power Output	0.67		3.50	dBm
DC Voltage		4.5		V
DC Current		0.06		A

4.2. Mixer Characterisation

In the heterodyne system, in order to decrease the resonant frequency (RF input) to intermediate frequency band a mixer is used. In this thesis a commercially available double balanced mixer (see Figure 4.14) that is designed for use in military, commercial and test equipment applications is used. The design of the mixer utilizes Schottky ring quad diodes and broadband soft dielectric and ferrite baluns. According to the datasheet some features of the mixer are:

Table 4.11. Some features of the Mixer

LO input port	7 to 15 GHz
RF input port	8 to 12.5 GHz
IF output port	DC to 2.5 GHz
LO drive	+10 dBm (nominal)
Peak input power	+23 dBm maximum at 25 °C

Characteristics of the mixer are examined by applying signals with various power and frequency supplied by two signal generators as LO and RF inputs (see Figure 4.15). IF output frequency spectrum and power are measured by using a spectrum analyzer. In order to investigate the IF output frequency spectrum and power, LO input signal is fixed to 12 GHz and 0 dBm, RF input signal is increased from 10 GHz to 11.75 GHz in 250

Figure 4.14. View of the commercially available mixer

MHz steps. At each frequency, power of the RF signal is also changed form -30 dBm to 0 dBm. Measurement results are illustrated in Figure 4.16 through Figure 4.23.
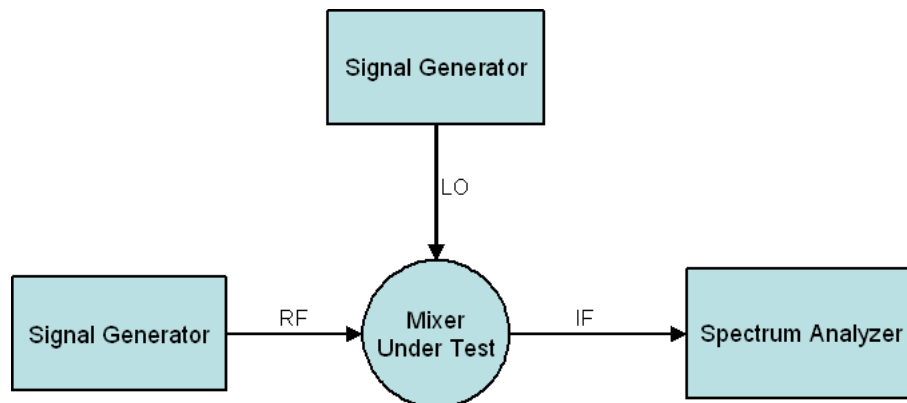
Figure 4.15. Intermediate frequency test setup

Initially, the frequency of the RF signal is set to 10 GHz and measurement results are obtained according to this case. For instance, in Figure 4.20 the wanted downconversion component (product of second order) is 1 GHz. The product of fourth order has higher power level than other higher order products, whereas the power level difference between the wanted frequency and the product of fourth order is 28 dB.

The output spectrum consists of the 1st harmonics, other higher order harmonics (2nd, 3rd, etc.), subharmonics and intermodulation products. As seen in Figure 4.16
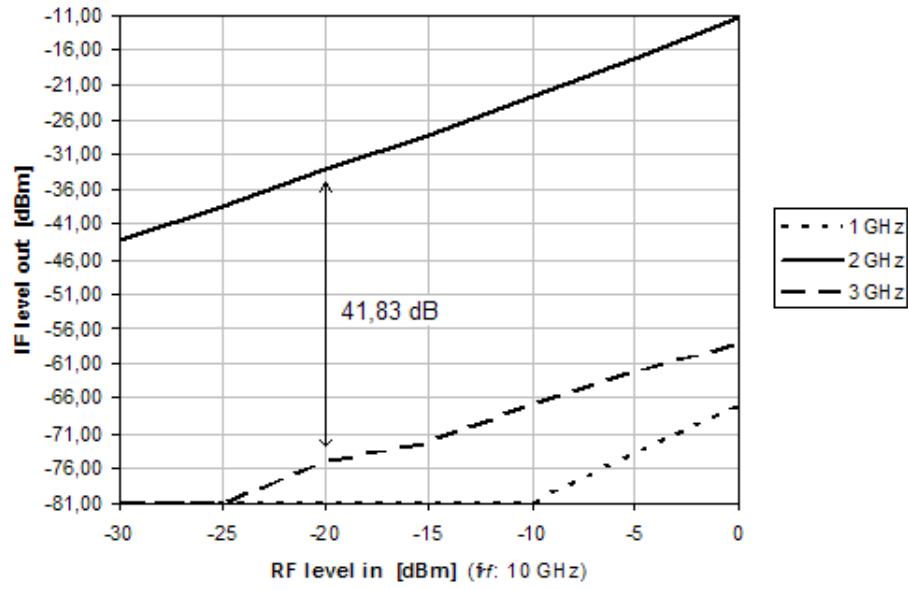
Figure 4.16. Intermediate frequency output spectrum where RF input is 10 GHz
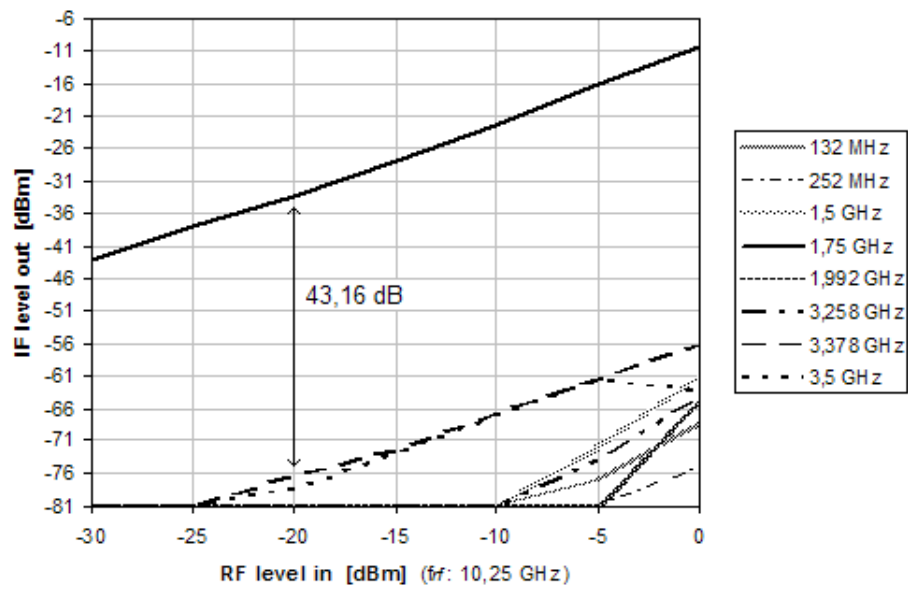
Figure 4.17. Intermediate frequency output spectrum where RF input is 10.25 GHz
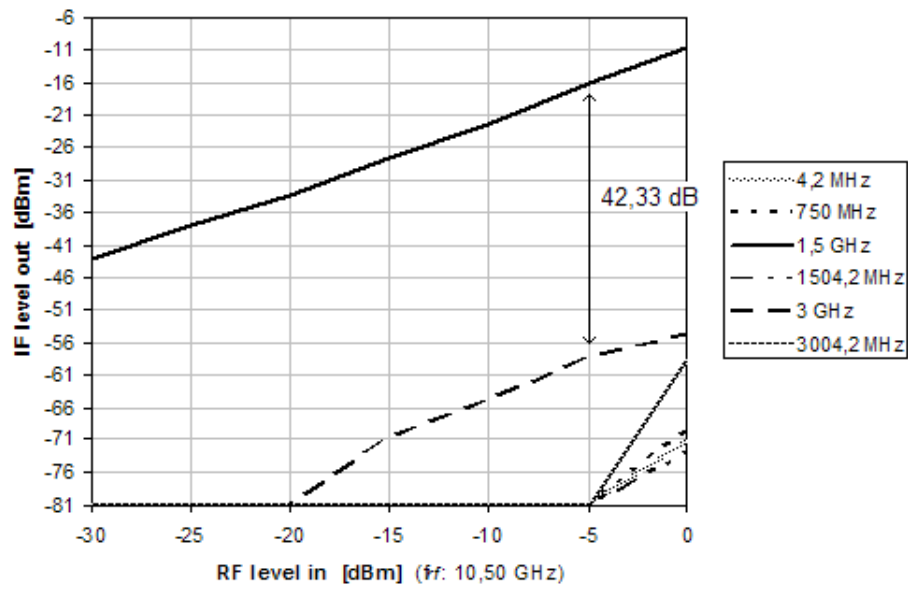
Figure 4.18. Intermediate frequency output spectrum where RF input is 10.50 GHz
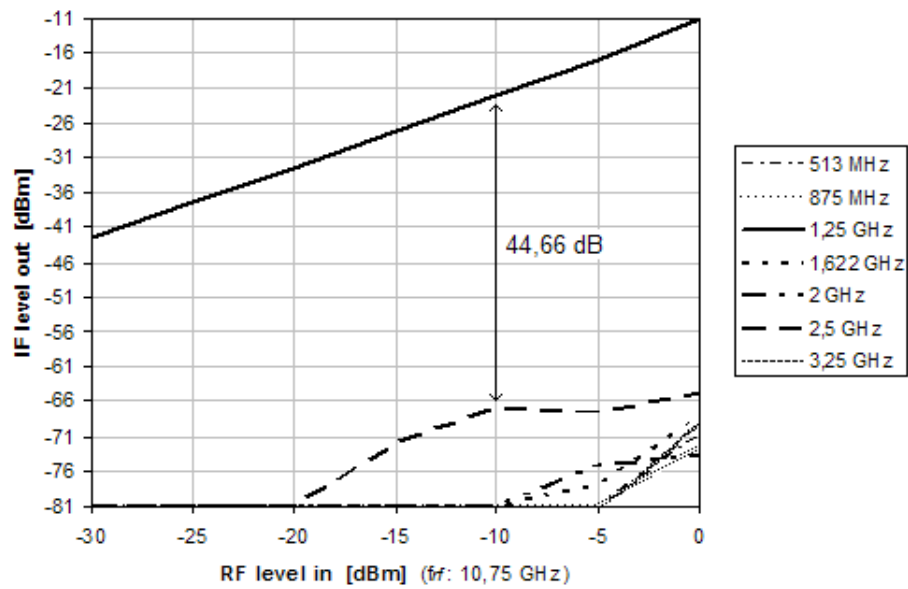
Figure 4.19. Intermediate frequency output spectrum where RF input is 10.75 GHz
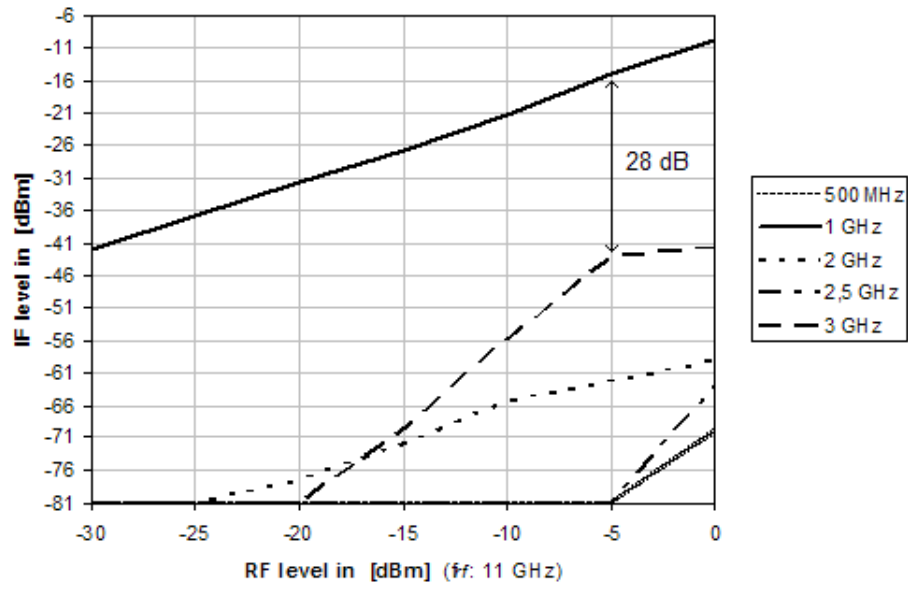
Figure 4.20. Intermediate frequency output spectrum where RF input is 11 GHz
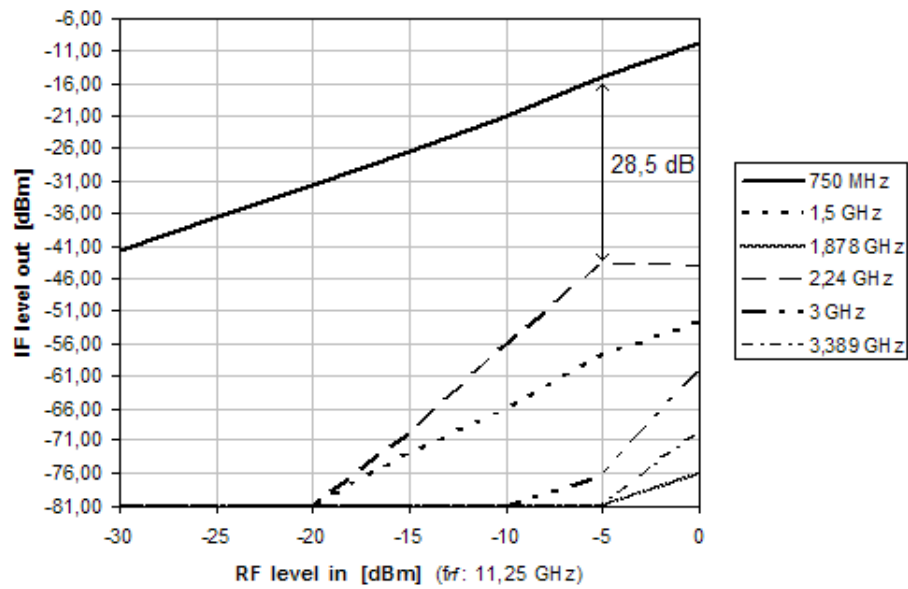
Figure 4.21. Intermediate frequency output spectrum where RF input is 11.25 GHz
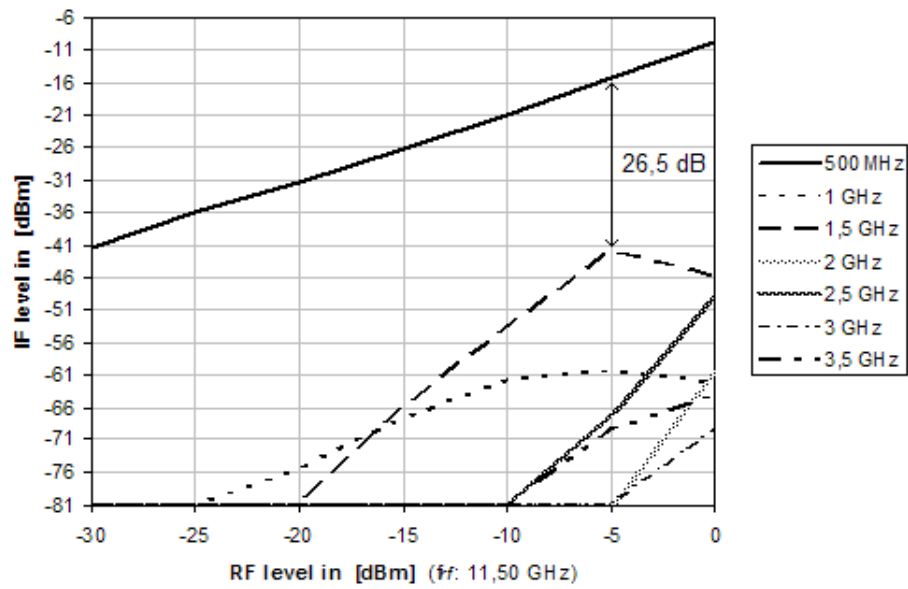
Figure 4.22. Intermediate frequency output spectrum where RF input is 11.50 GHz
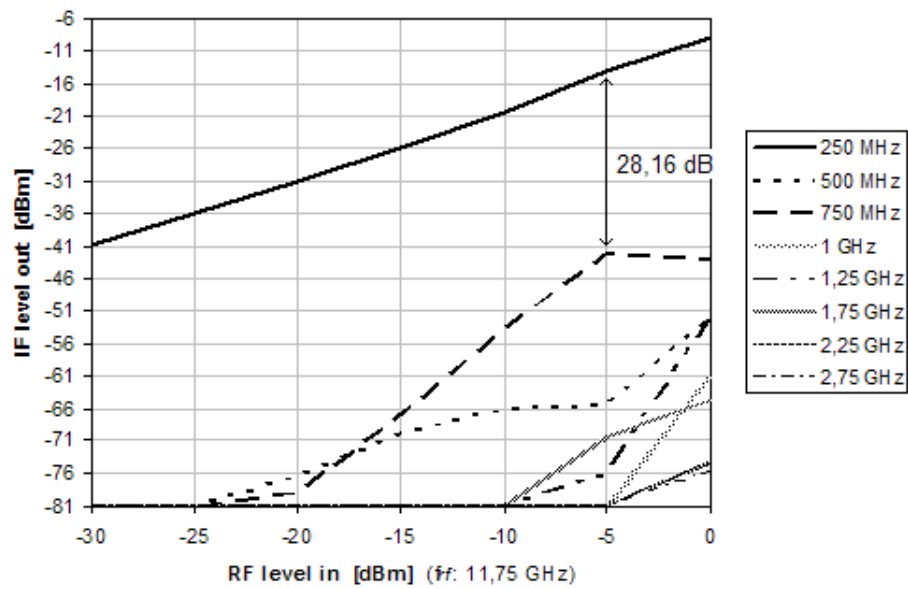
Figure 4.23. Intermediate frequency output spectrum where RF input is 11.75 GHz

through Figure 4.23, the minimum power level difference between the wanted frequency and higher order intermodulation products is 26.5 dB, whereas the noise floor level is -81 dBm. Since for good selectivity power difference between a wanted signal level and noise level should be greater than 10 dB, the mixer characteristics are satisfactory. As illustrated in Figure 4.16 through Figure 4.23, power levels of wanted frequencies are changed between -41 dBm to -11 dBm. As the LO input level is fixed to 0 dBm, power levels of the products increase as RF input level increases and vice versa.

4.3. IF Filter

As previously mentioned, a Chebyshev low-pass filter that has a 0.5 db passband ripple and 2.5 GHz cut off frequency is designed and realized using microstrip lines. As depicted in Figure 4.24 from (Ludwig and Bretchko 2001), the Chebyshev filter has the steepest slope at the cut-off region. This filter also has a passband ripple which can be controlled according to the design. Therefore, if a sharp transition from passband to stopband is necessary, ripples must be tolerated. Thus, the most proper choice would be the Chebyshev filter for this study.
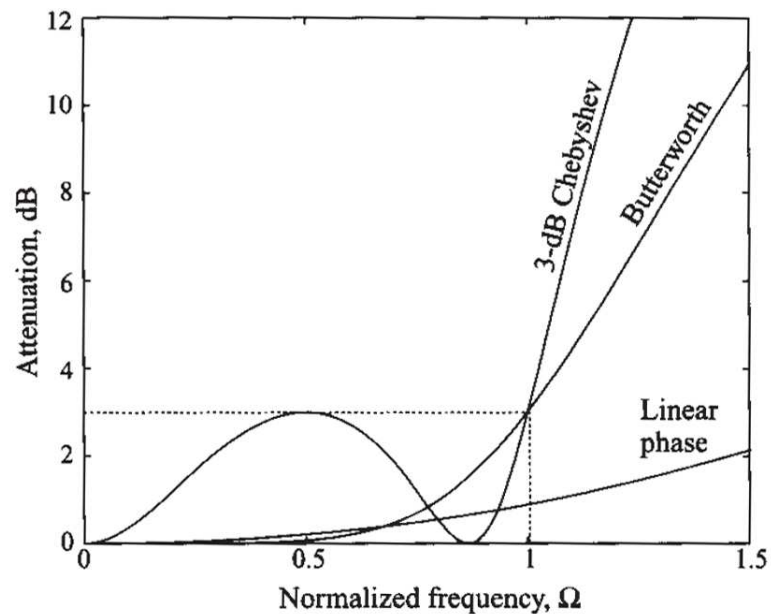
Figure 4.24. Comparison of the frequency response of the Butterworth, linear phase and Chebyshev 3rd order filters

4.3.1. Chebyshev-Type Filters

The design of the Chebyshev filter which is an equi-ripple filter type is based on an insertion loss whose profile is described by special polynomials named Chebyshev polynomials $T_N(\Omega)$. The insertion loss method allows a high degree of control over the passband and stopband amplitude and phase characteristics. The design trade-offs can be evaluated to satisfy the application requirements. For instance, if a minimum insertion loss is important, a Butterworth filter can be used. If a sharpest cut-off is required, Chebyshev filter will suit best for this case.

For the low-pass filter, the insertion loss (IL) is determined as

$$IL = 10\log\left(\frac{\text{Power available from source}}{\text{Power delivered to load}}\right) = 10\log\left(\frac{1}{1 - |\Gamma_{in}|^2}\right). \qquad (4.6)$$

Since $|\Gamma_{in}|^2$ is an even function of Ω, it can be represented as a polynomial in Ω^2.

$$|\Gamma_{in}|^2 = \frac{F(\Omega^2)}{F(\Omega^2) + G(\Omega^2)} \qquad (4.7)$$

where F and G are real polynomials in Ω^2. Substituting $|\Gamma_{in}|^2$ in Equation (4.6) the following relation is obtained:

$$IL = 10\log\left(1 + \frac{F(\Omega^2)}{G(\Omega^2)}\right) \qquad (4.8)$$

For a physically realizable filter its insertion loss must be in the form of Equation (4.8). Then, if a Chebyshev polynomial (Baez-Lopez and Ramirez-Cortes 1992) is used to represent the insertion loss of a low-pass filter, it becomes

$$IL = 10\log\{1 + a^2 T_N^2(\Omega)\} \qquad (4.9)$$

where

$$T_N(\Omega) = \cos\{N[\cos^{-1}(\Omega)]\}, \qquad \text{for} |\Omega| \leqslant 1$$
$$T_N(\Omega) = \cosh\{N[\cosh^{-1}(\Omega)]\}, \qquad \text{for} |\Omega| \geqslant 1$$

and Ω is the normalized frequency where $\Omega = \omega/\omega_c$ and N is the order of the filter. In order to see the behaviour of the Chebyshev polynomials, the first five terms are listed for the normalized frequency range of $-1 < \Omega < 1$:

$$T_0 = 1, \ T_1 = \Omega, \ T_2 = -1 + 2\Omega^2, \ T_3 = -3\Omega + 4\Omega^3, \ T_4 = 1 - 8\Omega^2 + 8\Omega^4$$

As seen from the polynomials, the first two terms are linear functions, and the rest terms are quadratic, cubic, and fourth-order functions, respectively (also see Figure 4.25).
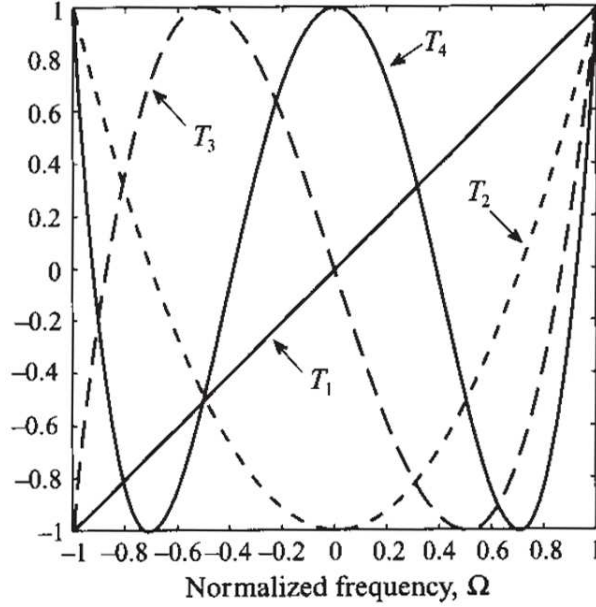
Figure 4.25. Chebyshev polynomials in the normalized frequency range $-1 \leqslant \Omega \leqslant 1$

Equi-ripple behaviour of the Chebyshev polynomial can be seen from the Figure 4.25, because all terms of the Chebyshev polynomial oscillate from -1 to +1 and that's why it is called equi-ripple behaviour. The magnitude of the transfer function $|H(j\Omega)|$ with Chebyshev polynomials is:

$$|H(\Omega)| = \sqrt{H(\Omega)H(\Omega)^*} = \frac{1}{\sqrt{1 + a^2 T_N^2(\Omega)}}, \qquad (4.10)$$

where a is a constant that controls the level of the passband ripples. If the variable a is chosen as $a = 1$ at $\Omega = 1$ due to $\omega = \omega_c$, the transfer function is

$$|H(1)| = \frac{1}{\sqrt{2}} = 0.707$$

which corresponds to the 3 db passband ripple. The frequency dependence of the insertion loss of the Chebyshev low-pass filter and the attenuation response of the Chebyshev filter with 3 db ripple are depicted in Figure 4.26 and Figure 4.27, respectively.

According to Figure 4.27, 3rd order filter design $N = 3$ is chosen for this study, and the level of 0.5 dB for the passband ripple is preferred. As mentioned above, since a
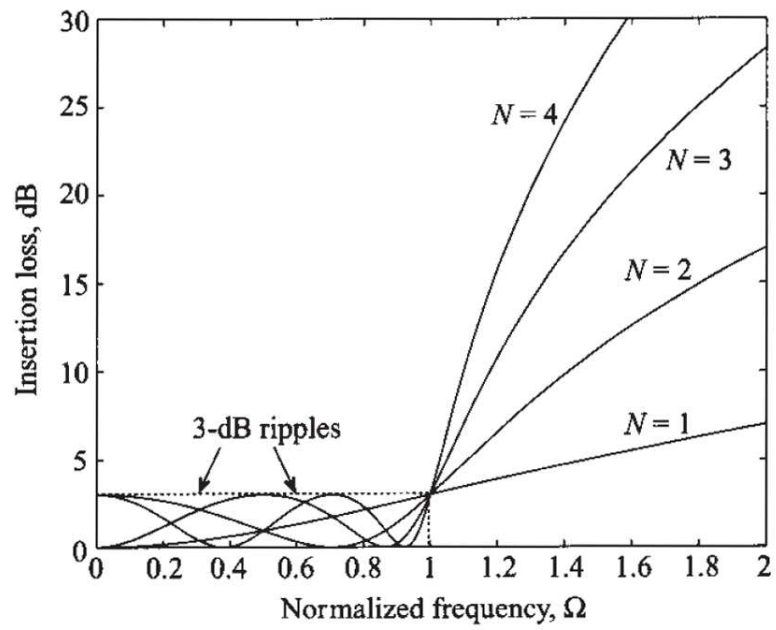
Figure 4.26. Normalized frequency versus insertion loss of the Chebyshev low-pass filter
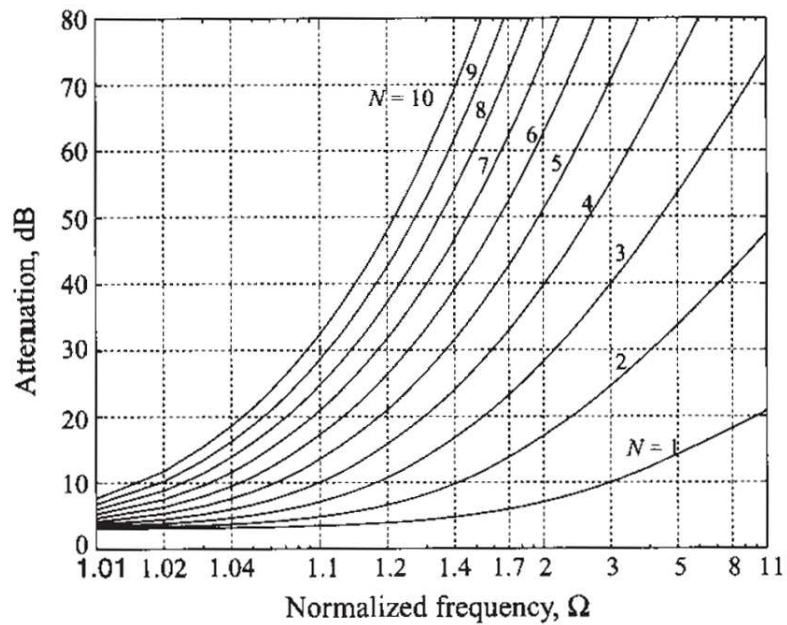
Figure 4.27. Attenuation response of 3 dB rippled Chebyshev filter

is a constant that controls the level of the passband ripples, it should be chosen according to Equation (4.11) that is derived from Equation (4.10) at $\Omega = 1$:

$$a = \sqrt{10^{\frac{RPL_{dB}}{10}} - 1} \quad , \tag{4.11}$$

where the desired level of the ripples is denoted by RPL_{dB}. In order to set the level of the ripple to 0.5 dB, a should be calculated as $a = \sqrt{10^{\frac{0.5}{10}} - 1} = 0.3493$. The attenuation for 0.5 dB Chebyshev filter is illustrated in Figure 4.28. When the Figures 4.27 and 4.28 are compared, it is clear that the drawback of a higher ripple in the passband has an advantage of a steeper transition to the stopband. As a result, 3rd order filter design with the level of 0.5 dB passband ripple has been chosen for this study.
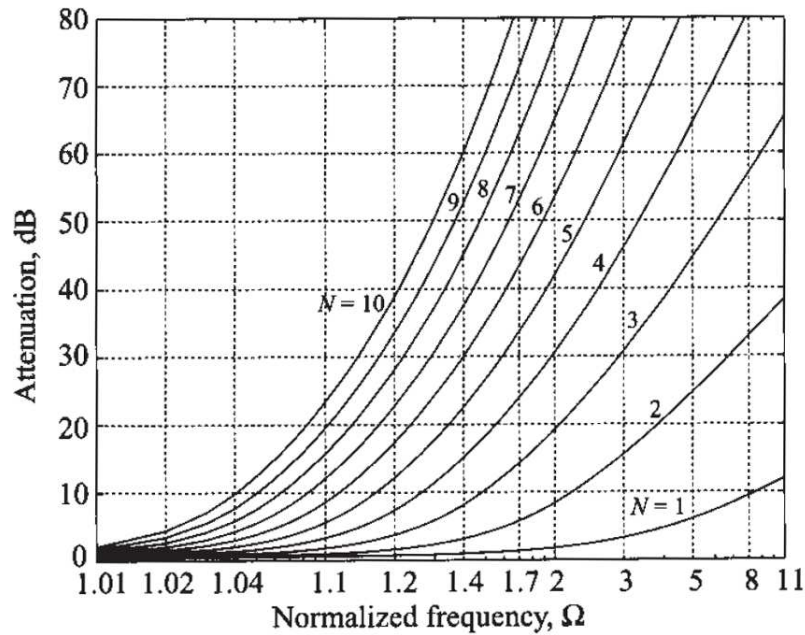
Figure 4.28. Attenuation of 0.5 dB rippled Chebyshev filter

Two type of normalized low-pass filter are depicted in Figure 4.29. The elements in the circuit are series inductance and shunt capacitance, and one follows the other. The aforementioned elements g are defined below:

$$g_0 = \begin{cases} \text{internal generator resistance for circuit in Figure 4.29 (a)} \\ \text{internal generator conductance for circuit in Figure 4.29 (b)} \end{cases}$$

45

$$g_m = \begin{cases} \text{inductance for series inductor} \\ \text{capacitance for shunt capacitor} \\ (m = 1, \ldots, N) \end{cases}$$

$$g_{N+1} = \begin{cases} \text{load resistance if the last element is a shunt capacitor} \\ \text{load conductance if the last element is a series inductor} \end{cases}$$
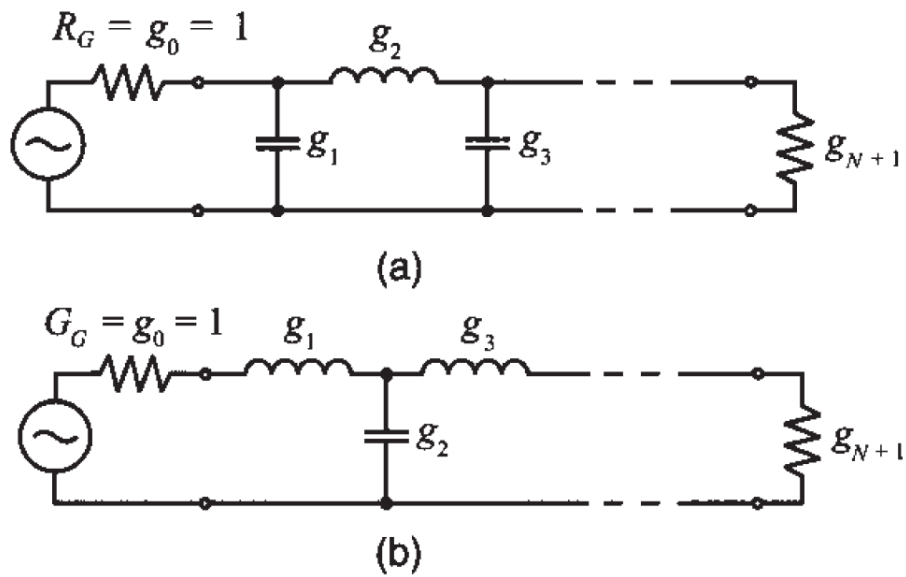
Figure 4.29. Two equivalent circuits of the low-pass filter with normalized elements

The aforementioned coefficients are listed in Table 4.12 for N up to 10 where $g_0 = 1$ and cut-off frequency $\omega_c = 1$.

Table 4.12. Chebyshev filter coefficients for 0.5 dB ripple level

N	g_1	g_2	g_3	g_4	g_5	g_6	g_7	g_8	g_9	g_{10}	g_{11}
1	0.6986	1.0000									
2	1.4029	0.7071	1.9841								
3	1.5963	1.0967	1.5963	1.0000							
4	1.6703	1.1926	2.3661	0.8419	1.9841						
5	1.7058	1.2296	2.5408	1.2296	1.7058	1.0000					
6	1.7254	1.2479	2.6064	1.3137	2.4758	0.8696	1.9841				
7	1.7372	1.2583	2.6381	1.3444	2.6381	1.2583	1.7372	1.0000			
8	1.7451	1.2647	2.6564	1.3590	2.6964	1.3389	2.5093	0.8796	1.9841		
9	1.7504	1.2690	2.6678	1.3673	2.7939	1.3673	2.6678	1.2690	1.7504	1.0000	
10	1.7543	1.2721	2.6754	1.3725	2.7392	1.3806	2.7231	1.3485	2.5239	0.8842	1.9841

4.3.2. Design of the Filter

Firstly, in order to design the filter, the aforementioned g_i values are denormalized to acquire the realistic frequency and impedance values according to the application requirements. It can be done in two steps: *Frequency transformation* and *Impedance transformation*.

Frequency transformation

Frequency transformation is the conversion of the normalized frequency Ω to the actual frequency ω. Thus, the cut-off frequency of the low-pass filter is scaled according to the application requirements. This transformation is composed of the scaling of the standart inductances and capacitances. For the inductive and capacitive elements normalized reactances are:

$$jX_L = j\Omega L \qquad (4.12)$$

$$jX_c = \frac{1}{j\Omega C} \qquad (4.13)$$

Since $\Omega = \omega / \omega_c$, Equation (4.12) and Equation (4.13) are written as:

$$jX_L = j\left(\frac{\omega}{\omega_c}\right)L = j\omega\tilde{L} \tag{4.14}$$

$$jX_c = \frac{1}{j(\frac{\omega}{\omega_c})C} = \frac{1}{j\omega\tilde{C}} \tag{4.15}$$

Thus, the actual inductance and capacitance values are

$$\tilde{L} = L/\omega_c \tag{4.16}$$

$$\tilde{C} = C/\omega_c. \tag{4.17}$$

Normalized inductance and capacitance L and C are determined by the coefficients g_i, and depend on the order of the filter or which equivalent circuit (see Figure 4.29) is preferred.

Impedance transformation

In the equivalent realizations of the filter illustrated in Figure 4.29 a unit source and a load resistance exist. However, the generator resistance g_0 and the load resistance R_L are not equal to unity. Therefore, those impedance coefficients should be scaled in order to meet the application requirements. As seen in Equation (4.18) through Equation (4.21), this objective is done by scaling all filter coefficients by the actual resistance R_G.

$$\bar{R}_G = 1 \cdot R_G \tag{4.18}$$

$$\bar{L} = LR_G \tag{4.19}$$

$$\bar{C} = \frac{C}{R_G} \tag{4.20}$$

$$\bar{R}_L = R_L R_G \tag{4.21}$$

where $\bar{R}_G$, $\bar{L}$, $\bar{C}$ and $\bar{R}_L$ are actual parameters, and L, C and R_L are the normalized values.

Design

As mentioned before, a 3rd order Chebyshev low-pass filter with 0.5 dB ripple is designed. Firstly, in order to do this, g coefficients are selected from the Table 4.12 according to the order $N = 3$. Coefficients are:

$$g_0 = 1.0000$$

$$g_1 = 1.5963$$

$$g_2 = 1.0967$$

$$g_3 = 1.5963$$

$$g_4 = 1.0000$$

where $R_G = g_0$, $L_1 = g_1$, $C_1 = g_2$, $L_2 = g_3$ and $R_L = g_4$ for the equivalent circuit of the filter. In other words, the design of the low-pass filter for this thesis is based on Figure 4.29 (b). The circuit with the normalized values is shown in Figure 4.30.
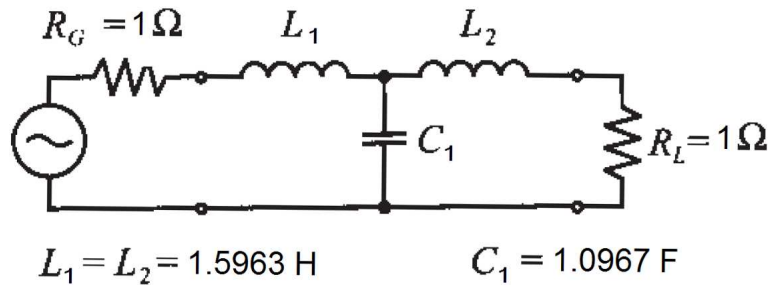
Figure 4.30. Lumped-element low-pass filter prototype with the normalized values

In this filter prototype both generator impedance R_G and load impedance R_L are assumed equal to unity. However, for this application the filter must be matched to a 50 Ω line impedance. Thus, scaling is applied as described by Equation (4.18) through Equation (4.21):

$$\bar{R}_G = 1 \times 50\,\Omega$$

$$\bar{L}_1 = 1.5963 \times 50 = 79.815\,\text{H}$$

$$\bar{C}_1 = \frac{1.0967}{50} = 21.934\,\text{mF}$$

$$\bar{L}_2 = 1.5963 \times 50 = 79.815\,\text{H}$$

$$\bar{R}_L = 1 \times 50\,\Omega$$

The filter structure with the element values normalized to 50 Ω is depicted in Figure 4.31.

$R_G = 50\,\Omega \quad L_1 \quad L_2$

$R_L = 50\,\Omega$

C_1

$L_1 = L_2 = 79.815\,\text{H} \qquad C_1 = 21.934\,\text{mF}$
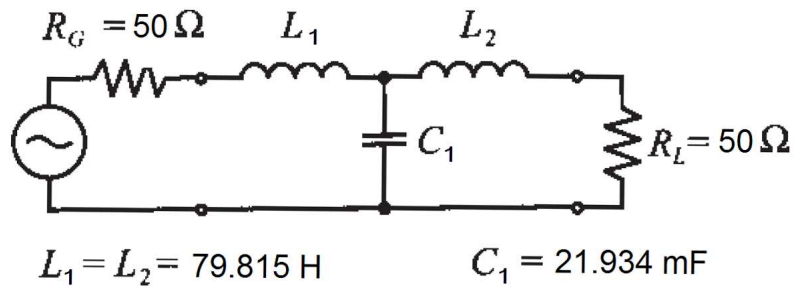
Figure 4.31. Lumped-element filter prototype after the impedance transformation

Although the element values are normalized to 50 Ω, the cut-off frequency of the filter is still 1 rad/s, i.e. $\omega_c = 1$ and therefore $f_c = 1/(2\pi) = 0.159$ Hz. Therefore, in order to get the true cut-off frequency, the frequency transformation is applied as the next step. As mentioned in Section 2, the cut-off frequency of the Chebyshev low-pass filter is set to 2.5 GHz. Applying the frequency transformation as described in Equation (4.16) and Equation (4.17) yields

$$\tilde{L}_1 = \frac{79.815}{2\pi 2.5 \times 10^9} = 5.081 \times 10^{-9} = 5.081\,\text{nH}$$

$$\tilde{C}_1 = \frac{21.934 \times 10^{-3}}{2\pi 2.5 \times 10^9} = 1.396 \times 10^{-12} = 1.396\,\text{pF}$$

$$\tilde{L}_2 = \frac{79.815}{2\pi 2.5 \times 10^9} = 5.081 \times 10^{-9} = 5.081\,\text{nH}$$

which are the actual inductive and capacitive values. As a result, the lumped-element low-pass filter that meets the application requirements is designed. The final circuit is shown in Figure 4.32.

$R_G = 50\,\Omega \quad L_1 \quad L_2$

$R_L = 50\,\Omega$

C_1

$L_1 = L_2 = 5.081\,\text{nH} \qquad C_1 = 1.396\,\text{pF}$
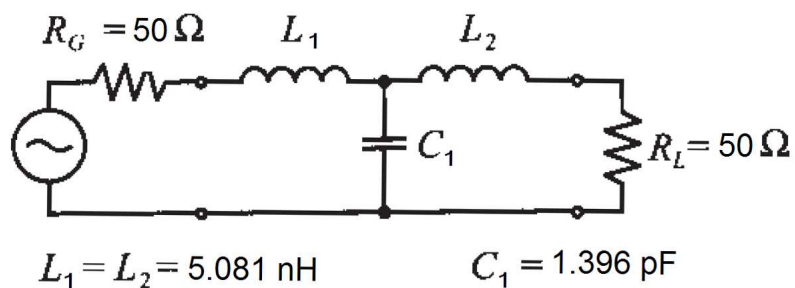
Figure 4.32. 0.5 dB rippled 3rd order Chebyshev low-pass filter whose cut-off frequency is 2.5 GHz

4.3.3. Microstrip Line Filter Implementation

Filter designs beyond 500 MHz are difficult to realize with lumped-elements, since the wave length of the signal becomes comparable with the size of the filter elements, and the elements can not be considered as lumped. In addition, at microwave frequencies losses become significant and reduce the performance of the filter circuit. Thus, to prevent this problem, the lumped-element filter designed previous subsection must be converted into distributed filter elements. In order to do this conversion, some tools are required like the Richards transformation (Richards 1948) and Kuroda's identities (Ludwig and Bretchko 2001). The Richards transformation is used to convert lumped-elements to transmission line sections and Kurodas identities are used to separate filter elements by using transmission sections. Such additional transmission line sections do not affect the filter response.

Richards transformation

Richards transformation is based on emulating the inductive and capacitive behaviour of the lumped-elements via open and short-circuit transmission line segments. The input impedance Z_{in} of a short-circuit transmission line ($Z_L = 0$ see Figure 4.33):

$$Z_{in} = jZ_0 \tan(\beta l) = jZ_0 \tan(\theta) \tag{4.22}$$

where $\beta = \omega/\nu_p$ is the phase constant and $\nu_p = 1/\sqrt{LC} = \lambda f$ is the phase velocity for lossless transmission lines. If the transmission line length l is taken as $\lambda_0/8$ at the frequency $f_0 = \nu_p/\lambda_0$, its electric length θ becomes

$$\theta = \beta \frac{\lambda_0}{8} = \frac{2\pi f}{\nu_p} \frac{\nu_p}{8 f_0} = \frac{\pi}{4} \Omega \tag{4.23}$$

where $\Omega = \omega/\omega_0$ is the normalized frequency.
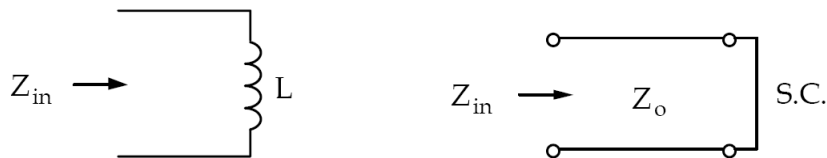
Figure 4.33. Input impedance of a short-circuit transmission line section and an inductive lumped-element

After substituting Equation (4.23) into Equation (4.22), the relation between the transmission line impedance and lumped-element impedance is obtained:

$$jX_L = j\omega L \equiv jZ_0 \tan\left(\frac{\pi}{4}\frac{f}{f_0}\right) = jZ_0 \tan\left(\frac{\pi}{4}\Omega\right) = SZ_0, \qquad (4.24)$$

where $S = j\tan(\pi\Omega/4)$ is the Richards transform. In a similar way, a capacitive lumped-element can be represented by an open-circuit transmission line section (see Figure 4.34). The input impedance Z_{in} of a open-circuit transmission line is

$$Z_{in} = \frac{Z_0}{j\tan(\beta l)} = \frac{Z_0}{j\tan(\theta)}. \qquad (4.25)$$

Figure 4.34. Input impedance of an open-circuit transmission line section and a capacitive lumped-element

And the relation between the transmission line impedance and lumped-element impedance is

$$jB_C = j\omega C \equiv jY_0 tan\left(\frac{\pi}{4}\Omega\right) = SY_0 \qquad (4.26)$$

where Y_0 is the admittance and B_C is the capacitive suseptance. Thus, by using the Richards transformation, lumped inductors can be replaced with short-circuit lines of the characteristic impedance $Z_0 = L$, and capacitors with open-circuit lines of the characteristic impedance $Z_0 = 1/C$ (see Figure 4.35).

For the transmission line length l, the value $l = \lambda_0/8$ is used. Instead of $\lambda_0/8$ also $\lambda_0/4$ could be used as line length but $\lambda_0/8$ is more convenient to perform. Because $S = j1$ at the cut-off frequency $f = f_0 = f_c$ so the transformation is simpler. Furthermore, the size of the designed circuit by using $\lambda_0/8$ lines is smaller than for $\lambda_0/4$.

The drawback is that the Richards transformation limits the lumped-element response from $0 \leq f \leq \infty$ to $0 \leq f \leq 4f_0$ because of the periodic behaviour of the tangent function and considering the line length of $\lambda_0/8$. Furthermore, due to the behaviour of the tangent function in order to obtain the inductive responses, the frequency interval is
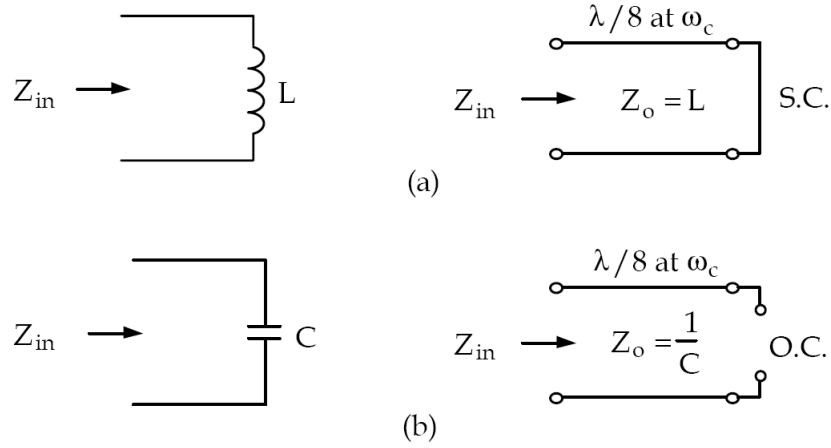
Figure 4.35. Richards transformation (a) For an inductor to a short-circuit line

(b) For a capacitor to an open-circuit line

limited to $0 \leq f \leq 2f_0$. Therefore, such kind of filter is not a broadband filter.

Unit elements

In order to form practically realizable transformations it is necessary to separate the transmission line elements. This procedure is performed by inserting unit elements (UEs). The electric length of the unit element is $\theta = \dfrac{\pi}{4}(f/f_0)$ and the characteristic impedance is Z_{UE}. Thus, the transmission line representation of the unit element by ABCD parameters is

$$[\mathbf{UE}] = \begin{bmatrix} A_{UE} & B_{UE} \\ C_{UE} & D_{UE} \end{bmatrix} = \begin{bmatrix} cos(\theta) & jZ_{UE}sin(\theta) \\ \dfrac{jsin(\theta)}{Z_{UE}} & cos(\theta) \end{bmatrix} = \dfrac{1}{\sqrt{1-S^2}} \begin{bmatrix} 1 & Z_{UE}S \\ \dfrac{S}{Z_{UE}} & 1 \end{bmatrix}.$$

Kuroda's identities

Kuroda's identities simplify the conversion of a given filter implementation to a more suitable filter realization. For example, it is more complicated to realize a series inductance by a short-circuit transmission line segment than a shunt stub line. Therefore, in order to make easier this process, Kuroda's identities summarized in Figure 4.36 are used. Thus, Kuroda's identities have three aims: First, to separate transmission line segments physically. Second, to transform series stubs into shunt stubs, or vice versa. And third, to change impractical characteristic impedances into more realizable ones.

Initial Circuit	Kuroda's Identity

$$N = 1 + Z_2/Z_1$$
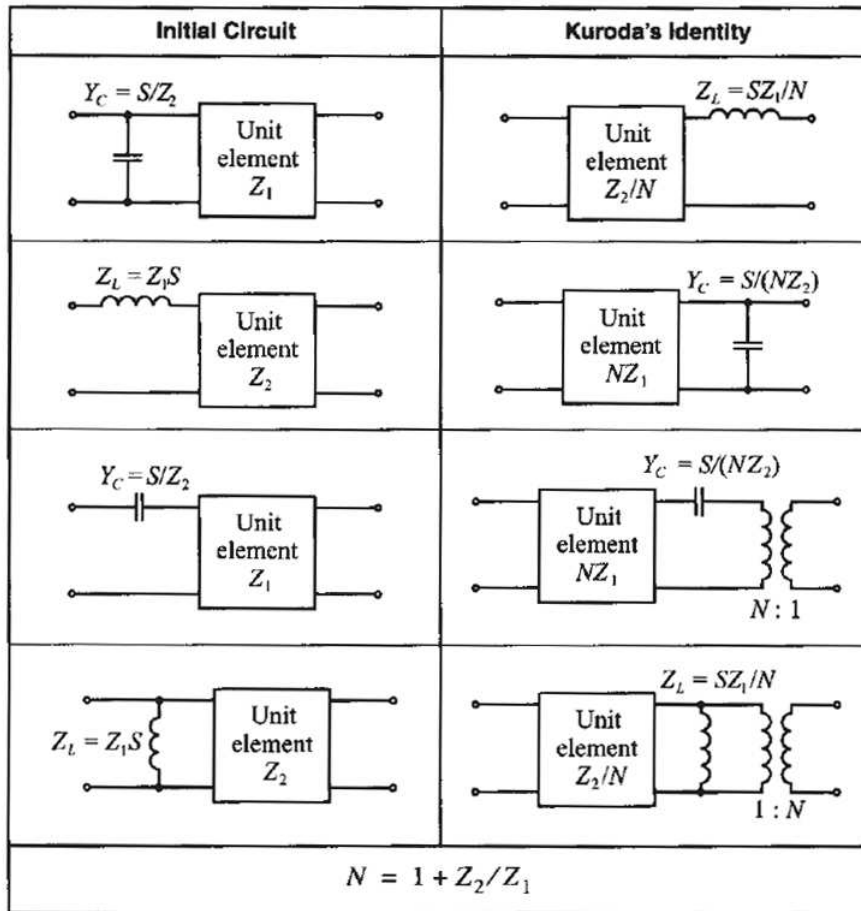
Figure 4.36. Kuroda's identities

Microstrip filter design

As discussed before the normalized low-pass prototype element values are

$$g_0 = 1.0000$$
$$g_1 = 1.5963$$
$$g_2 = 1.0967$$
$$g_3 = 1.5963$$
$$g_4 = 1.0000$$

where $R_G = g_0$, $L_1 = g_1$, $C_1 = g_2$, $L_2 = g_3$ and $R_L = g_4$ (see Figure 4.30). To convert series inductors to short-circuited lines and shunt capacitors to open-circuited lines the Richards transformation is performed as shown in Figure 4.37. According to the transformation the characteristic impedance of a short-circuited line is L and the characteristic impedance of an open-circuited line is $1/C$, respectively. As mentioned before all lines are $\lambda_0/8$ long.
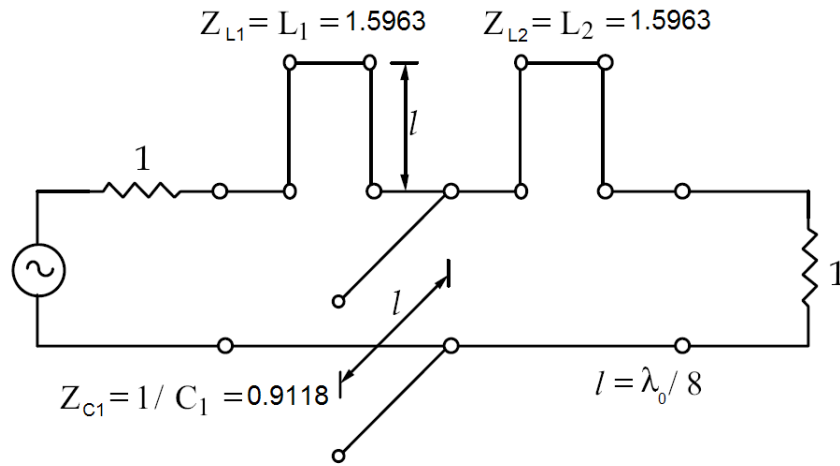
Figure 4.37. Performing Richards transformation to convert inductors and capacitor to short-circuited and open-circuited lines

The short-circuited lines depicted in Figure 4.37 are difficult to implement in microstrip line form because of nonideal via. Therefore, to convert those lines to shunt stubs Kuroda's identities are used. Firstly, unit elements are added to the begining and end of the filter as shown in Figure 4.38.
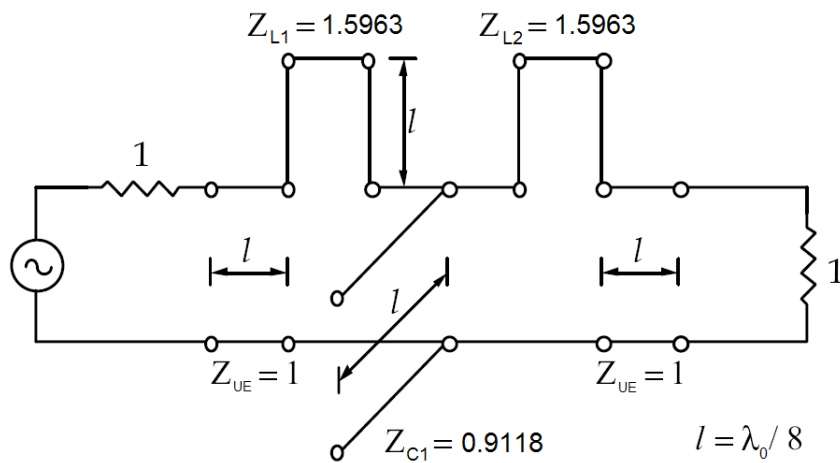
Figure 4.38. Adding unit elements

Unit elements ($Z_{UE} = 1$) do not effect filter performance because they are matched to the source and load and assumed lossless. Thus, after the unit elements are added, Kuroda's identities can be applied. The value for N whose equation is shown in Figure 4.36 and then the denormalized impedance values are calculated as

$$N = 1 + Z_2/Z_1 = 1 + Z_{UE}/Z_{L1} = 1 + \frac{1}{1.5963} = 1.6265$$

$$Z_{NL1} = NZ_{L1} = 1.6265 \times 1.5963 = 2.5964$$

$$Z_{NL2} = NZ_{L2} = 1.6265 \times 1.5963 = 2.5964$$

$$Z_{NUE} = NZ_{UE} = 1.6265 \times 1 = 1.6265 \,.$$

Then, the second Kuroda's identity is applied as illustrated in Figure 4.39.
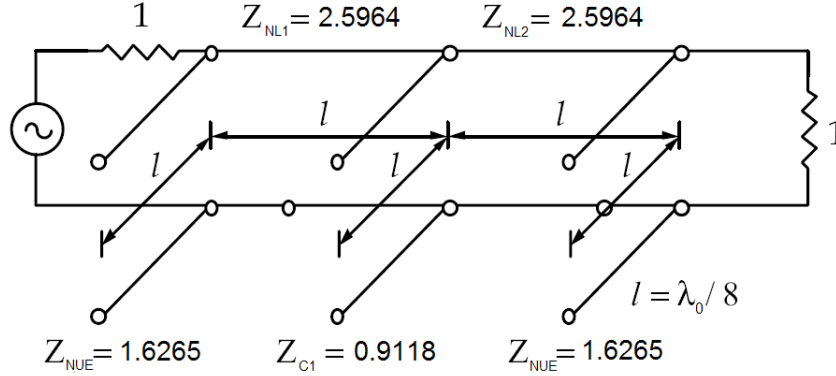
Figure 4.39. Appliying the second Kuroda's identity

Now, the next step is to scale impedance and frequency. The impedance scaling is done by multiplying the normalized characteristic impedances by 50 Ω as in Equation (4.18) through Equation (4.21):

$$\bar{Z}_G = 50\,\Omega$$

$$\bar{Z}_{UE} = 50 \times 1.6265 = 81.33\,\Omega$$

$$\bar{Z}_{L1} = 50 \times 2.5964 = 129.82\,\Omega$$

$$\bar{Z}_{L2} = 50 \times 2.5964 = 129.82\,\Omega$$

$$\bar{Z}_{C1} = 50 \times 0.9118 = 45.59\,\Omega$$

Choosing line and stub lengths as $\lambda_0/8$ at the cut-off frequency of 2.5 GHz results in frequency scaling. The result of impedance and frequency scaling is depicted in Figure 4.40.

Finally, the width w of the microstrip line (see figure 3.7) and the height of the dielectric material h are calculated according to the Equation (3.2). By using Figure 4.41, the ratio w/h is estimated according to the dielectric constant of the used dielectric material and characteristic line impedance. As a dielectric material, the FR4 substrate is
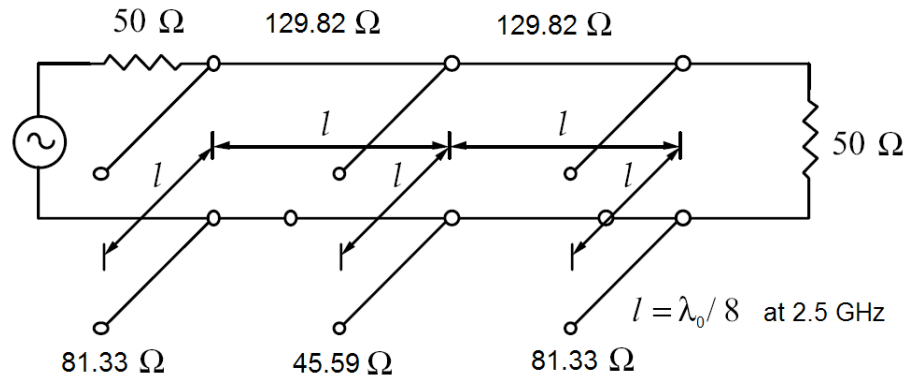
Figure 4.40. After impedance and frequency scaling

used with the dielectric constant of $\varepsilon_r = 4.7$ and the height of $h = 1.5$ mm. The thickness of the microstrip line is $t = 0.035$ mm and made of copper.
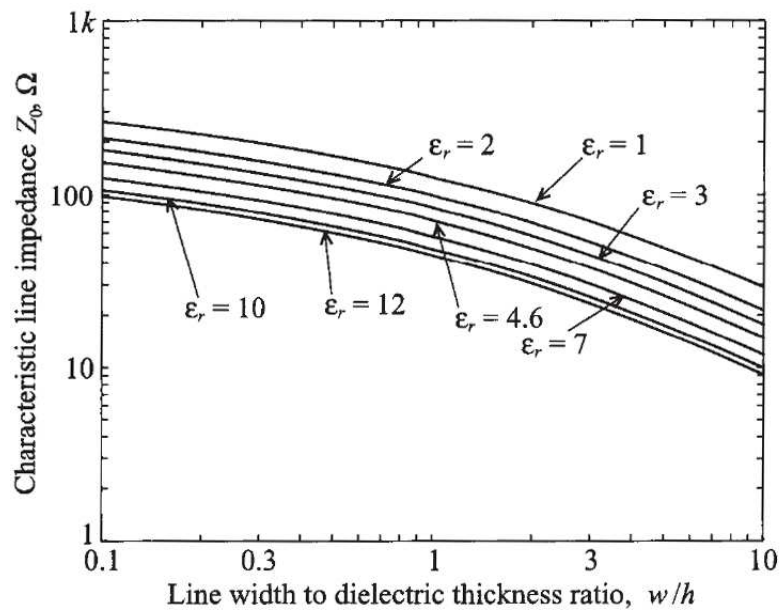
Figure 4.41. Characteristic line impedance as a function of w/h

Thus, Equation (3.2) for $w/h \leq 1$ is used to calculate the width of the microstrip line w for the characteristic line impedances $\bar{Z}_{UE} = 81.33\ \Omega$ and $\bar{Z}_{L1} = \bar{Z}_{L2} = 129.82\ \Omega$ and Equation (3.2) for $w/h > 1$ is used for the $\bar{Z}_G = 50\ \Omega$ and $\bar{Z}_{C1} = 45.59\ \Omega$. In order to obtain accurate w values, computer codes are designed for each characteristic line impedance. The estimated w/h values from the Figure 4.41 as presented for instance in (Ludwig and Bretchko 2001) are used for the first iteration. Then, by using these codes

57

the width of the each line is computed. Furthermore, according to the effective dielectric constant $\varepsilon_{r,eff}$, the length l of each line is calculated. In the following, the calculations steps for all transmission lines are presented.

45.59 Ω Stub:

$w/h = 2.132$

Therefore, $w = 3.1980$ mm

$$func(w/h) = \frac{1}{\sqrt{1 + 12/2.132}} = 0.3884 \text{ for } w/h > 1$$

$$\varepsilon_{r,eff} = \frac{4.7 + 1}{2} + \frac{4.7 - 1}{2} \times 0.3884 = 3.5686$$

$$Z_{msl} = \frac{376.8}{\sqrt{\varepsilon_{r,eff}}}[2.132 + 1.393 + 0.667 \times ln(2.132 + 1.444)]^{-1} = 45.5926 \text{ Ω}$$

The speed of light in a dielectric medium is $\nu_p = c/\sqrt{\varepsilon_{r,eff}}$, the wavelength is $\lambda = \nu_p/f$, and with $l = \lambda/8$ we obtain the length $l = \dfrac{c}{8f\sqrt{\varepsilon_{r,eff}}}$ where c is the speed of light in vacuum.

Therefore, $l = \dfrac{c}{8 \times 2.5 \times 10^9 \sqrt{3.5686}} = 7.9349$ mm

50 Ω Stub:

$w/h = 1.831$

Therefore, $w = 2.7465$ mm

$$func(w/h) = \frac{1}{\sqrt{1 + 12/1.831}} = 0.3638 \text{ for } w/h > 1$$

$$\varepsilon_{r,eff} = \frac{4.7 + 1}{2} + \frac{4.7 - 1}{2} \times 0.3638 = 3.5231$$

$$Z_{msl} = \frac{376.8}{\sqrt{\varepsilon_{r,eff}}}[1.831 + 1.393 + 0.667 \times ln(1.831 + 1.444)]^{-1} = 49.9957 \text{ Ω}$$

$$l = \frac{c}{8 \times 2.5 \times 10^9 \sqrt{3.5231}} = 7.9860 \text{ mm}$$

81.33 Ω Stub:

$w/h = 0.694$

Therefore, $w = 1.0410$ mm

$$func(w/h) = \frac{1}{\sqrt{1 + 12/0.694}} + 0.04(1 - 0.694)^2 = 0.2376 \text{ for } w/h \leq 1$$

$$\varepsilon_{r,eff} = \frac{4.7 + 1}{2} + \frac{4.7 - 1}{2} \times 0.2376 = 3.2895$$

$$Z_{msl} = \frac{376.8}{2\pi\sqrt{3.2895}}ln(\tfrac{8}{0.694} + 0.25 \times 0.694) = 81.3284 \text{ Ω}$$

$$l = \frac{c}{8 \times 2.5 \times 10^9 \sqrt{3.2895}} = 8.2647 \text{ mm}$$

<u>129.82 Ω Stub:</u>

$w/h = 0.175$

Therefore, $w = 0.2625$ mm

$$func(w/h) = \frac{1}{\sqrt{1 + 12/0.175}} + 0.04(1 - 0.175)^2 = 0.1471 \text{ for } w/h \leq 1$$

$$\varepsilon_{r,eff} = \frac{4.7 + 1}{2} + \frac{4.7 - 1}{2} \times 0.1471 = 3.1222$$

$$Z_{msl} = \frac{376.8}{2\pi\sqrt{3.1222}} ln(\tfrac{8}{0.175} + 0.25 \times 0.175) = 129.7625 \ \Omega$$

$$l = \frac{c}{8 \times 2.5 \times 10^9 \sqrt{3.1222}} = 8.2647 \text{ mm}$$

Thus, the resulting microstrip filter illustrated in Figure 4.42 is implemented using the values obtained above. In addition, the microstrip lines are connected by T-junctions.
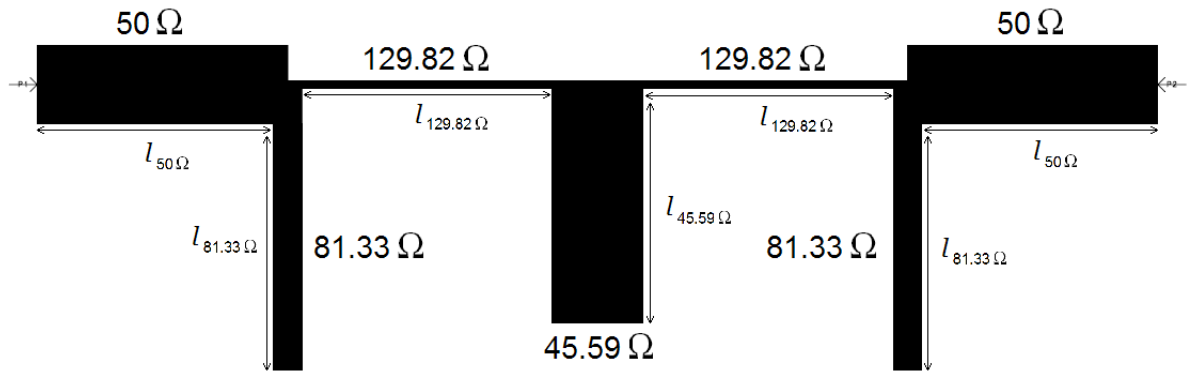
Figure 4.42. Resulting microstrip low-pass filter

Figure 4.42 is drawn as a layout by using a commercially available electronic design software. In order to test the performance of the 0.5 dB microstrip line low-pass Chebyshev filter, the microstrip filter design is simulated using a commercially available simulation tool, based on the method of moments. Figure 4.43 depicts the simulated forward transmission S_{21} of the designed microstrip line filter using the calculated values.

As seen from Figure 4.43, the designed low-pass filter shows Chebyshev low-pass filter characteristic. The ripple in the passband is approximately 0.5 dB, however the 3 dB cut-off frequency of 2.6 GHz is somewhat higher than the desired frequency of 2.5 GHz. In order to obtain the desired cut-off frequency (2.5 GHz), the designed filter is tuned by adjusting the physical dimensions of the microstrip stubs. Therefore, the lengths l of the microstrip stubs are increased by 5 % in order to set the cut-off frequency to 2.5 GHz. The S_{21} forward transmission of the low-pass filter using tuned values is depicted in Figure
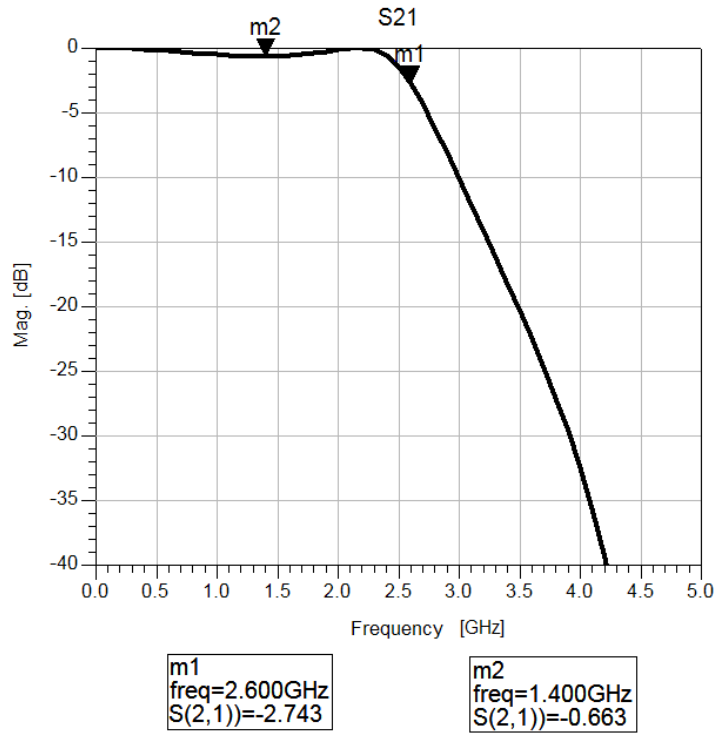
Figure 4.43. S_{21} system response simulation of the designed microstrip line filter

4.44. It can be seen from the Figure 4.44 that the cut-off frequency is at the desired value of 2.5 GHz.

However, because of the limited precision of the fabrication process of the designed microstrip low-pass filter, the width and the tuned length values must be rounded off until the first digit after the decimal point. Figure 4.45 shows the S_{21} system response of the filter after rounding off the w and l values given in Table 4.13.

Table 4.13. Final width and length values of each microstrip stub

	Length [mm]	Width [mm]
45.59 Ω	8.3	3.2
50 Ω	8.4	2.8
81.33 Ω	8.7	1
129.82 Ω	8.9	0.3

Finally, the designed microstrip line filter is fabricated (see Figure 4.46) and then
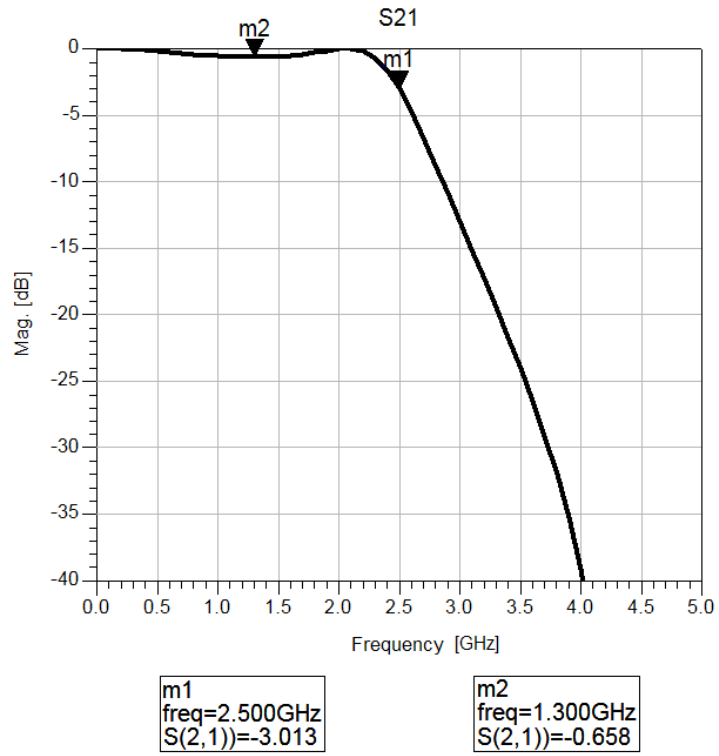
Figure 4.44. S_{21} system response simulation of the tuned microstrip line filter
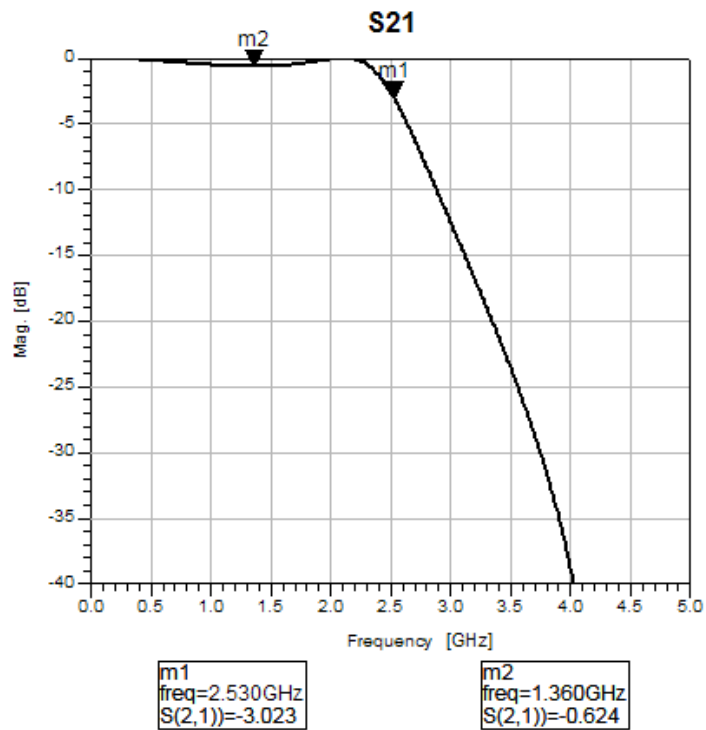
Figure 4.45. S_{21} system response simulation of the designed microstrip line filter
after rounding off

tested by using a network analyzer. The transmission plot in Figure 4.47 shows that, cut-off frequency of the realized microstrip line low-pass filter is 2.599 GHz, which is 99 MHz higher than simulated. The higher -1.018 dB passband ripple of Chebyshev filter is due to losses of both the conductor and the dielectric material, but is acceptable. As for the high frequency ripples on the system response, they may be due to the multiple reflections between the microstrip stubs or because of the unsymmetrical geometry of the stubs. As a result, fabricated microstrip line low-pass filter meets the requirements of the designed microstrip line low-pass Chebyshev filter.
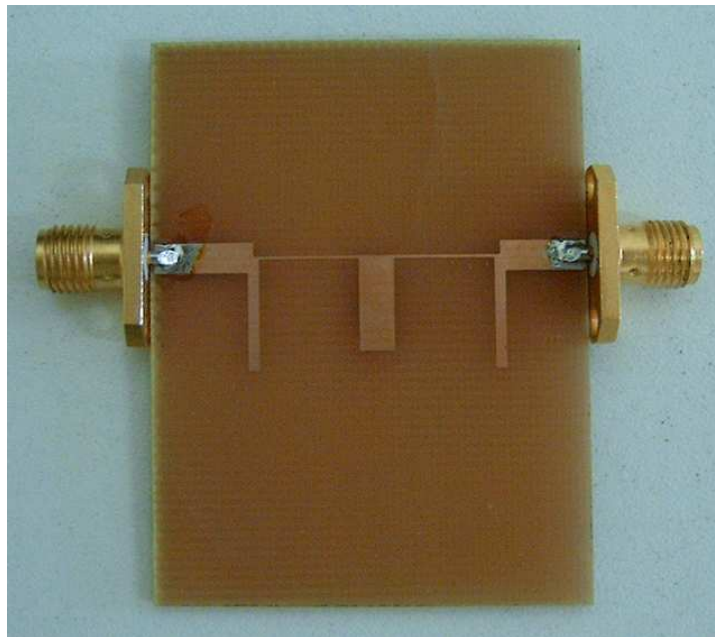
Figure 4.46. Fabricated microstrip line low-pass filter
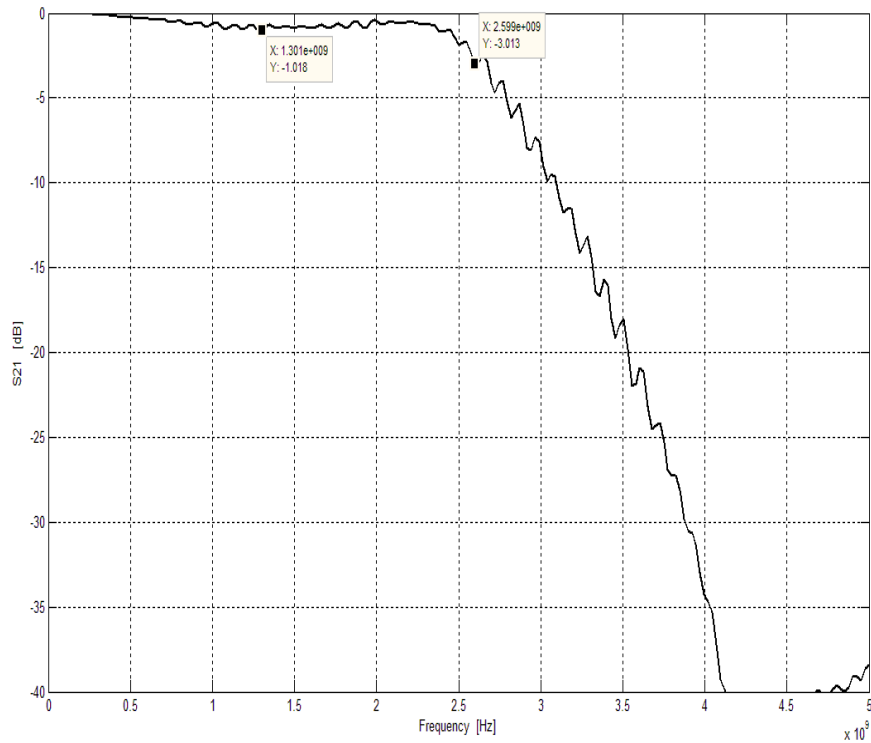
Figure 4.47. Measured S_{21} system response of the realized microstrip line filter

4.4. Frequency Counter Tests

In the receiver system, the commercially available frequency counter Tecstar FC-2500 is used. The FC-2500, shown in Figure 4.48, is a microprocessor controlled precision universal frequency counter. The frequency range is between 5 Hz and 2.5 GHz. Typical measurement functions include frequency, period, ratio, pulse width and count. Input A is a high impedance input (1 MΩ) for frequencies ranging from 5 Hz to 25 MHz. Input B is a 50 Ω input for the frequencies ranging from 20 MHz to 2.5 GHz. Seven significant digits of result are produced per second. The instrument includes an RS-232 serial interface allowing remote control by a computer. Specifications of the instrument are shown in Tables 4.14 and 4.15.

Since the frequency spectrum of the intermediate frequency ranges from 100 MHz to 2500 MHz port B (20 MHz - 2500 MHz, 50 Ω) of the FC-2500 is used.

Table 4.14. Measurement range - Port A

Frequency	5 Hz to 25 MHz
Sensitivity (sine wave)	Max $20\,\mathrm{mV_{rms}}$ 15 Hz to 25 MHz Typically $5\,\mathrm{mV_{rms}}$ Pulse $50\,\mathrm{mV}$ 0 Hz to 25 MHz
Impedance	$1\,\mathrm{M\Omega}\,//\,25\,\mathrm{pF}$
Maximum input voltage	$50\,\mathrm{V_{rms}}$ 5 Hz to 50 Hz $1\,\mathrm{V_{rms}}$ 50 Hz to 25 MHz
Accuracy	+/-1 count, +/-1 time base accuracy

Table 4.15. Measurement range - Port B

Frequency	20 MHz to 2500 MHz
Sensitivity	Max $50\,\mathrm{mV_{rms}}$ 20 MHz to 2500 MHz Typically $15\,\mathrm{mV_{rms}}$
Impedance	$50\,\Omega$ nominal
Maximum input voltage	$1\,\mathrm{V_{rms}}$ 20 MHz to 2500 MHz
Accuracy	+/-1 count, +/-1 time base accuracy

Figure 4.48. View of the commercially available frequency counter

4.4.1. Power Limitations on the Frequency Measurement Boundaries

In order to test the frequency range accuracy according to the power of the input signal, a signal generator is directly connected to the FC-2500 (see Figure 4.49), and the frequency of the signal is measured for various power levels.
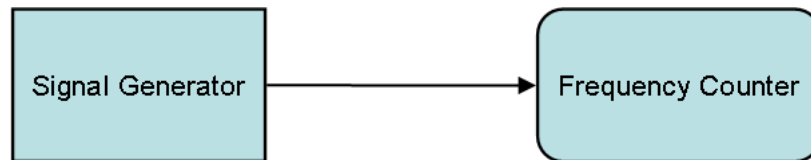
Figure 4.49. Frequency measurement accuracy test setup

The test is performed for two frequencies: the lowest frequency that port B of the FC-2500 can measure (20 MHz) and the highest frequency that port B of the FC-2500 can measure (2500 MHz). To get more detailed information and to discuss the measurement results of the FC-2500, a spectrum analyzer is additionally used. The measurement results are listed in Table 4.16.

Table 4.16. Frequency measurement accuracy test

Signal power	Signal frequency	Frequency measurement (via spectrum analyzer)	Frequency measurement (via FC-2500)
-5 dBm	20 MHz	20.0 MHz	20.00003 MHz
-8 dBm	20 MHz	20.0 MHz	20.00048 MHz
-8.40 dBm	20 MHz	20.0 MHz	20.00094 MHz
-9 dBm	20 MHz	20.0 MHz	20.00237 MHz
-20 dBm	2.5 GHz	2.50 GHz	2500.0037 MHz
-15.40 dBm	2.5 GHz	2.50 GHz	2500.0036 MHz
-15.30 dBm	2.5 GHz	2.50 GHz	2499.9527 MHz

As seen in Table 4.16, the power level of the signal is decreased from -8 dBm to -9 dBm for the 20 MHz test and increased from -20 dBm to -15.30 dBm for the 2500 MHz test. For signal levels higher than - 5 dBm, there is no change in the frequency measure-

ment. As a result, at the frequency 20 MHz the measurement error increases significantly for power levels smaller than -8 dBm. At the frequency 2500 MHz, the measurement error increases significantly for power levels larger than -15.40 dBm. Therefore, for the accurate measurement the input power level should be greater than or equal to -8 dBm at 20 MHz and less than or equal to -15.40 dBm at 2500 MHz. Between 25 MHz and 2500 MHz the highest allowed level of the input signal is 1 V_{rms}. This corresponds to +13.01 dBm for an impedance of 50 Ω. The lowest level of the input signal should be typically 15 mV_{rms}, which corresponds to -23.47 dBm for an impedance of 50 Ω. Results are shown in Table 4.17.

Table 4.17. Power limitations on the frequency measurement boundaries

at 20 MHz	$P_{in} \geqslant -8\,\mathrm{dBm}$
at 2500 MHz	$P_{in} \leqslant -15.40\,\mathrm{dBm}$
$20\,\mathrm{MHz} < f_{in} < 2500\,\mathrm{MHz}$	$-23.47\,\mathrm{dBm} \leqslant P_{in} \leqslant 13.01\,\mathrm{dBm}$

4.5. Data Conversion

In this study, a circular groove guide oscillator is used as a microwave sensor and distance measurement is performed by the oscillator connected to the heterodyne system. Figure 4.50 shows the simulated output spectrum of the circular groove guide oscillator according to the distance between its plates. The frequency shift of about 250 MHz is depicted in 1 mm steps as the distance is increased from 13 mm to 16 mm.

Equation (4.27) gives the relation of f_{res} the resonant frequency of the oscillator in GHz and d the distance between its plates in mm. This frequency-to-distance equation is derived by using polynomial curve fitting algorithm as represented in (Darlington 1990, Draper and Smith 1998). The derivation process is performed by a computer code, and as a data set for regression, the simulated data of the oscillator is used. For each different sensor new equations are obtained as the calibration process. According to the equation given below, the increment of the distance in 1 mm steps cause the frequency shift of about 267 MHz.

$$d = -3.7327 f_{res} + 46.6166 \tag{4.27}$$
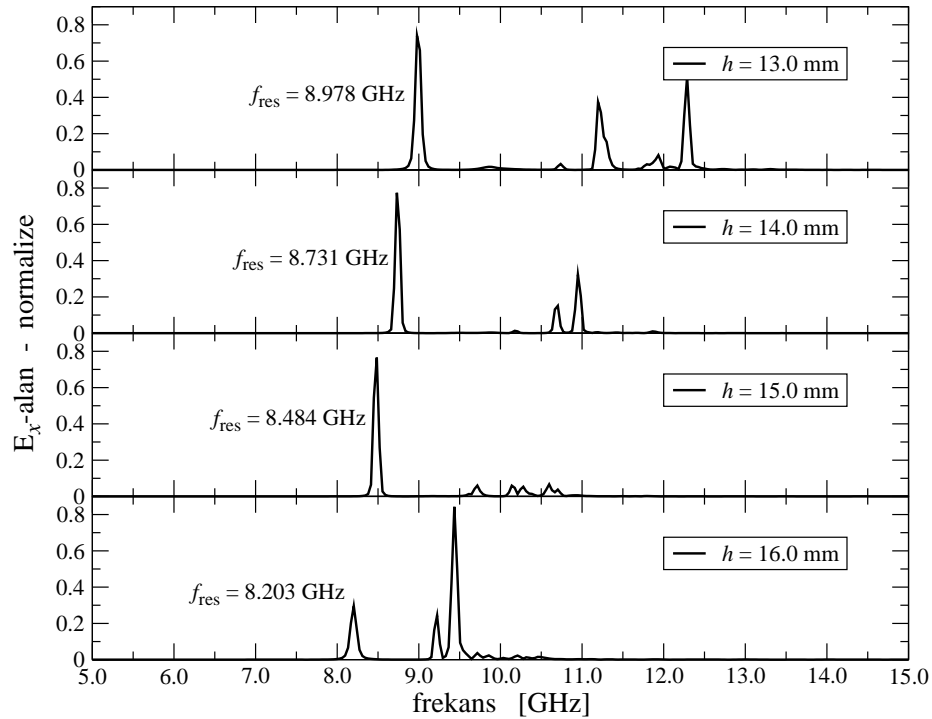
Figure 4.50. The simulated output spectrum of the oscillator

In Figure 4.51, the plus signs show the simulation results of the oscillator with respect to the resonant frequency and the distance between the plates. The solid line is the plot of the frequency-to-distance equation which is given above.

The frequency data is received from the frequency counter by a computer via RS232 protocol to convert the frequency data to distance. Thus, the equation which is used to obtain the distance data is

$$d = -3.7327(f_{VCO} - f_{IF}) + 46.6166 \,, \tag{4.28}$$

where f_{VCO} is the frequency of the VCO and f_{IF} is the received frequency from the frequency counter.

As listed in Table 4.18, the maximum expected error is 104 μm due to the curve fitting. The data conversion process can be robust if a lookup table is prepared rather than estimating the distance value by Equation (4.28). Lookup table is formed by using the measured frequency values of the oscillator for each distance value with desired steps.

Table 4.18. Obtained distance values and errors

| Resonant Frequency [GHz] (simulated)	Distance [mm] (obtained)	Error [μm]
8.978	13.1042	104.2134
8.942	13.2386	-11.4084
8.872	13.4999	-0.1175
8.802	13.7612	11.1735
8.731	14.0262	26.1972
8.661	14.2875	37.4881
8.625	14.4219	-78.1337
8.555	14.6832	-66.8427
8.484	14.9482	-51.8190
8.414	15.2095	-40.5281
8.344	15.4708	-29.2371
8.273	15.7358	-14.2135
8.203	15.9971	-2.9225
8.133	16.2584	8.3684
8.062	16.5234	23.3921
7.992	16.7847	34.6831
7.921	17.0497	49.7068
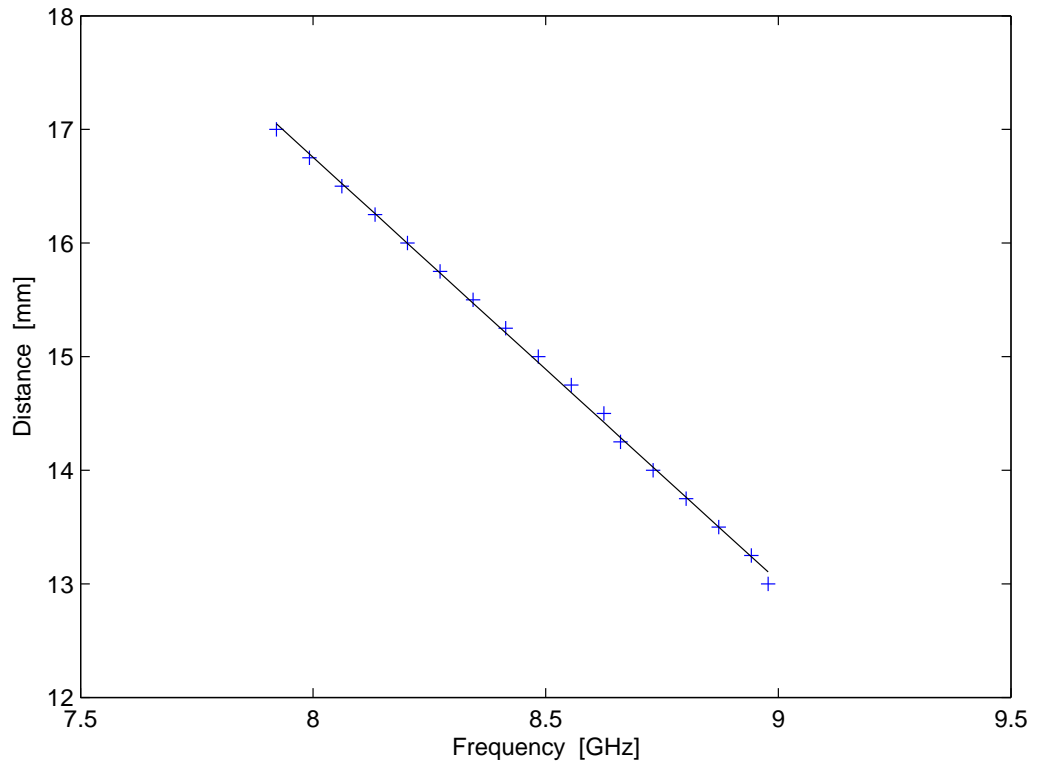
Figure 4.51. The plot of the frequency-to-distance equation

CHAPTER 5

CONCLUSION

In this study, heterodyne receiver system is set up and calibrated to measure the resonant frequencies of resonator type sensors precisely and inexpensively. Output frequencies of the resonator type sensors are varied by the change in physical dimensions of the resonator or physical properties of a material placed in a resonator to be processed. Instead of the classical radio amplifier and a loudspeaker a frequency counter evaluates the signal. Thus, the heterodyne receiver used for frequency measurement consists of a mixer, a voltage controlled oscillator, a microstrip line low-pass filter and a frequency counter operating up to 2.5 GHz.

Characteristics of the mixer are examined by applying signals with various power levels and frequencies supplied by two signal generators as LO and RF inputs. Output frequency of the IF signal and power are measured via a spectrum analyzer. Characterisation of the VCO is done by determining supply voltage, measuring output frequency and output power according to tuning voltage, and measuring phase noise. The frequency range of the counter according to the power of the input signal is determined as frequency counter test. VCO and mixer characterisation, and frequency counter test show that the mixer, the VCO and the frequency counter, which are used in the heterodyne system, are appropriate for frequency measurement system. Furthermore, a microstrip line low-pass filter which is a 3rd order Chebyshev filter with 0.5 dB passband ripple is designed and realized in order to suppress any frequency apart from intermediate frequency. The simulation result of the designed filter and measurement result of the realized filter are almost matched.

Distance measurement is performed by using a circular groove guide oscillator as a microwave sensor connected to the heterodyne receiver system. To calibrate the system for distance measurement, the simulation data of the oscillator is used. As the future work of this study, dielectric constant measurement is the initial aim. Since the output frequency of the groove guide oscillator is varied by the physical properties of a material put in to the groove guide resonator, the oscillator connected to the frequency measurement system can be utilized for dielectric constant measurement. In order to do this, the heterodyne

receiver system should be calibrated to measure the dielectric constant of a material.

REFERENCES

Armstrong, E. H. 1921. A new system of Short Wave Amplification. *Proceedings of the IRE* 9: 3-11.

Armstrong, E. H. 1924. The Super-Heterodyne-Its Origin, Development, and Some Recent Improvements. *Proceedings of the IRE* 12: 539-552.

Vertiy, A. A., Gavrilov, S. P., Aydinlik, S. and Samedov S. 1996. Circular groove shaped resonator for millimeter waves. *International Journal of Infrared and Millimeter Waves* 17 (10): 1613-1637.

Baez-Lopez, D. J. M. and J. M. Ramirez-Cortes. 1992. Direct determination of the coefficients of Chebyshev polynomials and other considerations. *Proceedings of the 35th Midwest Symposium on Circuits and Systems* 1: 466-468.

Bechteler, A. S. A. and L. Sevgi. 2004. Millimeter Waveband SemiSymmetrical Groove Guide Resonators. *IEEE Microwave Magazine* 5 (3): 51-60.

Bechteler, Thomas F. 2004. *Microwave Measurement Techniques.* Izmir: IYTE course script.

Bechteler, Thomas F. 2004. *Microwave Devices and Applications.* Izmir: IYTE course script.

Bechteler, T. F., Kustepeli, A. and Bechteler, S. A. 2008. Design of coupling structures for groove guide resonators. *Microwave and Optical Technology Letters* 50 (5): 1406-1410.

Carullo, A., Ferrero, A. and Parvis, M. 1999. A microwave system for relative humidity measurement. *Instrumentation and Measurement Technology Conference:IMTC/99* 1: 124-129.

Darlington, Richard B. 1990. *Regression and Linear Models.* Singapore: McGraw-Hill.

Draper, Norman R. and Harry Smith. 1998. *Applied Regression Analysis.* New York: John Wiley & Sons.

Godara, L. C. 1999. Introduction to the Heterodyne Receiving System, and Notes on the Recent Arlington-Salem Tests. *Proceedings of the IEEE* 87: 1975-1978.

Hammerstad, E. O. 1975. Equations for Microstrip Circuit Design. *5th European Microwave Conference* 268-272.

Hammerstad, E. O. and ϕ. Jensen. 1980. Accurate Models for Microstrip Computer-Aided Design. *IEEE MTT-S Int. Microwave Symp. Dig.* 407-409.

Henderson, Bert C. 1990. *Mixers in Microwave Systems (Part 2).* California. Watkins-Johnson Company. http://www.wj.com (accessed April 26, 2008).

Hewlett-Packard Company. Test and Measurement Center. 1997. *Fundamentals of Quartz Oscillators.* Englewood: Hewlett-Packard Company.

Komiyama, B., Kiyokawa, M. and Matsui, T. 1991. Open resonator for precision dielectric measurements in the 100 GHz band. *IEEE Transactions on Microwave Theory and Techniques* 39 (10): 1792-1796.

Ludwig, Reinhold and Pavel Bretchko. 2001. *RF Circuit Design - Theory and Applications.* New Jersey: Prentice Hall.

Megej, A., Beilenhoff, K., Schussler, M., Ziroff, A., Mottet, B., Yilmazoglu, O., Mutamba, K., Hamann, C.D., Baican, R. and Hartnagel, H.L. 2002. Integrated microwave sensors for cavity-length measurement in machine engineering. *IEEE Transactions on Microwave Theory and Techniques* 50 (12): 3070-3076.

Pavio, A. M., Halladay, R. H., Bingham, S. D. and Sapashe, C. A. 1988. Double balanced mixers using active and passive techniques. *IEEE Transactions on Microwave Theory and Techniques* 36 (12): 1948-1957.

Richards, P. I. 1948. Resistor-Transmission-Line Circuits. *Proceedings of the IRE* 36 (2): 217-220.

Thumm, Manfred and Werner Wiesbeck, eds. 1998. *Hochfrequenzmetechnik - Verfahren und Mesysteme.* Leipzig: B. G. Teubner.